J. Fluid Mech. (2014), *vol.* 743, *pp.* 295–326. © Cambridge University Press 2014
doi:10.1017/jfm.2014.35

Water entry without surface seal: extended cavity formation

M. M. Mansoor[1], J. O. Marston[1,†], I. U. Vakarelski[1,2] and S. T. Thoroddsen[1,2]

[1]Division of Physical Sciences and Engineering, King Abdullah University of Science and Technology, Thuwal 23955-6900, Saudi Arabia

[2]Clean Combustion Research Centre, King Abdullah University of Science and Technology, Thuwal 23955-6900, Saudi Arabia

(Received 22 June 2013; revised 22 October 2013; accepted 10 January 2014; first published online 4 March 2014)

We report results from an experimental study of cavity formation during the impact of superhydrophobic spheres onto water. Using a simple splash-guard mechanism, we block the spray emerging during initial contact from closing thus eliminating the phenomenon known as 'surface seal', which typically occurs at Froude numbers $Fr = V_0^2/(gR_0) = O(100)$. As such, we are able to observe the evolution of a smooth cavity in a more extended parameter space than has been achieved in previous studies. Furthermore, by systematically varying the tank size and sphere diameter, we examine the influence of increasing wall effects on these guarded impact cavities and note the formation of surface undulations with wavelength $\lambda = O(10)$ cm and acoustic waves $\lambda_a = O(D_0)$ along the cavity interface, which produce multiple pinch-off points. Acoustic waves are initiated by pressure perturbations, which themselves are generated by the primary cavity pinch-off. Using high-speed particle image velocimetry (PIV) techniques we study the bulk fluid flow for the most constrained geometry and show the larger undulations ($\lambda = O(10$ cm$)$) have a fixed nature with respect to the lab frame. We show that previously deduced scalings for the normalized (primary) pinch-off location (ratio of pinch-off depth to sphere depth at pinch-off time), $H_p/H = 1/2$, and pinch-off time, $\tau \propto (R_0/g)^{1/2}$, do not hold for these extended cavities in the presence of strong wall effects (sphere-to-tank diameter ratio), $\epsilon = D_0/D_{tank} \gtrsim 1/16$. Instead, we find multiple distinct regimes for values of H_p/H as the observed undulations are induced above the first pinch-off point as the impact speed increases. We also report observations of 'kinked' pinch-off points and the suppression of downward facing jets in the presence of wall effects. Surprisingly, upward facing jets emanating from first cavity pinch-off points evolve into a 'flat' structure at high impact speeds, both in the presence and absence of wall effects.

Key words: cavitation, high-speed flow, jets

1. Introduction

The cavity formation produced by water entry of spheres can be related to the cavity formation produced by water entry of torpedoes (May & Hoover 1963),

† Email address for correspondence: jeremy.marston@kaust.edu.sa

https://doi.org/10.1017/jfm.2014.35 Published online by Cambridge University Press

skipping of boats (Rosellini *et al.* 2005), dip-coating procedures (Burley 1992) and the motion of lizards that appear to walk on water (Glasheen & McMahon 1996). Worthington & Cole (1897, 1900) and Worthington (1908) were the first to investigate cavity formation and splash characteristics produced by spheres impacting onto liquid surfaces using single-spark illumination photography. Following their work, Mallock (1918), Bell (1924) and Ramsauer & Dobke (1927) provided further descriptions of the observed cavity characteristics, while the first sets of quantitative results were presented by Gilbarg & Anderson (1948), Richardson (1948), May & Woodhull (1948, 1950) and May (1951, 1952) who collectively investigated sphere impacts with water surfaces, highlighting the influence of atmospheric pressure, overall impact forces involved and the effect of the sphere wettability on the observed cavity and splash characteristics.

With further developments in high-speed imaging technology (Thoroddsen, Etoh & Takehara 2008) and theoretical models, recent studies have lead to better understanding of transient cavity dynamics in the context of sphere surface condition. Duez *et al.* (2007) investigated the effect of sphere wettability and liquid properties on the threshold velocity (U^*) of cavity entrainment. Here U^* was identified to be independent of the static contact angle θ_0 in the wetting regime ($\theta_0 < 90^0$) and decreased rapidly in the non-wetting regime ($\theta_0 > 90^0$). For a given θ_0, U^* was found to be proportional to the capillary velocity (σ_{LV}/μ_L), where σ_{LV} is the liquid–vapour surface tension and μ_L is the liquid viscosity. At impact velocities above the entrainment value, Duclaux *et al.* (2007) proposed two different analytical models, one constraining the cavity radial velocity to zero (relevant to cavities created by long cylinders) and the other having a non-zero radial cavity velocity (applicable to those created by spheres). Analytical models were found to be in fair agreement with experimental results. For spheres which do not decelerate significantly during fall, the evolution of the reduced depth location (H/R_0), the reduced crater size (R/R_0) and the reduced pinch-off location (H_p/H) as a function of the Froude number $Fr = V_0^2/(gR_0)$ were found to be $H/R_0 \approx Fr^{1/2}$, $R/R_0 \approx Fr^{1/4}$ and $H_p/H = 1/2$, respectively. Investigating cavity collapse at low Bond numbers $Bo = (\rho g R_0^2)/\sigma \in [10^{-2}, 10]$, where surface tension effects are no longer negligible, Aristoff & Bush (2009) identified four different cavity types as the Weber number $We = (\rho V_0^2 R_0)/\sigma$ was increased in the range $10^{-1} < We < 10^3$ and categorized them into quasi-static, shallow seal, deep seal and surface seal regimes. The possibility of simultaneous dual pinch-offs was shown for $We = O(100)$, whilst consecutive multiple pinch-offs (each generating an air capsule of a smaller volume than the preceding one) was also observed for $We \approx 400$ in the surface seal regime. A complete non-wetting entry was observed by Marston, Vakarelski & Thoroddsen (2012*a*) who investigated the impact of 'Leidenfrost spheres' (see also Vakarelski *et al.* 2011), whereby the temperature of the impacting sphere exceeded the Leidenfrost temperature of the liquid. While cold spheres formed no cavities at low impact speeds, Leidenfrost spheres were reported to produce extremely smooth cavities due to the absence of a contact line. If the sphere temperature was lowered or the impact speed increased, a dual cavity structure was obtained due to a short period of physical contact at the equator of the sphere. No discernible difference was obtained in cavities produced by cold and Leidenfrost spheres at high impact speeds.

In addition to these studies, other notable works pertaining to water entry include that of Shi, Itoh & Takami (2000), who analysed supercavitation induced by high-speed water entry of projectiles at 342 m s^{-1} and identified the '*pull-away*' of the cavity beneath the water surface. Gekle *et al.* (2008) demonstrated the unique effect

https://doi.org/10.1017/jfm.2014.35 Published online by Cambridge University Press

of capillary ripples on cavity dynamics to result in two asymptotic regimes separated by discrete jumps for the scaled pinch-off depths with respect to the Froude number, hence proving the non-universality of cavity collapse. Gekle *et al.* (2010) showed that the air flow inside collapsing cavities can achieve supersonic speeds which affected the cavity shape in the final stages of pinch-off producing a marked '*kink*' and an upward motion of the necking region prior to pinch-off. Gekle *et al.* (2009) further highlighted the importance of radial energy concentrated along the cavity walls which collide to drive flow at the base of these Worthington jets. Thoroddsen *et al.* (2004) investigated the initial stages of impact between a solid sphere and liquid surface and found the emission of a high-speed horizontal jet immediately after initial contact, which was shown to be a significant source of energy dissipation in the water entry phenomenon. Marston, Vakarelski & Thoroddsen (2011) demonstrated the existence of a small volume of air entrapped between the bottom tip of the impacting sphere and the liquid free surface. This air pocket peeled sideways at low impact Reynolds numbers but contracted at $Re \geqslant 1000$ to form a bubble. Truscott & Techet (2009) examined the impact of spinning spheres and found the formation of a fluid wedge across the centre of an asymmetrical cavity. Aristoff *et al.* (2010) investigated the deceleration of spheres with a broad range of densities and found the pinch-off depths, total cavity depths and pinch-off times to decrease as the sphere density decreased.

When a hydrophobized sphere impacts a water surface beyond a certain impact velocity or equivalently Froude number $Fr = V_0^2/(gR_0)$, the air flow into the resulting cavity can be strong enough to suck together the splash crown above the surface. The splash sheet then converges along the axis of symmetry, which is known as the '*surface seal*'. Droplets from the seal then enter and collide with the cavity interface formed beneath the liquid surface, distorting the cavity walls (May 1952) thus making it difficult to examine the pinch-off depths in this regime. This phenomenon naturally inhibited previous experimental studies from investigating cavity closure depths at high Froude numbers ($Fr > 100$) (i.e. in the early surface seal region) and instead have resorted to theoretical (Birkhoff & Isaacs 1951) and numerical methods (Bergmann *et al.* 2009). Recent experimental results for the pinch-off depth versus Froude number by Duclaux *et al.* (2007) in this regime were measured with a high degree of scatter, which possibly dissuaded them from obtaining results at higher Froude numbers ($Fr >$ 300). Using an analytical model, the reduced neck location was concluded to have a constant value of 0.5. For the Leidenfrost sphere impacts, Marston *et al.* (2012*a*) also reported a scatter in scaled pinch-off depths in the early surface seal regime ($Fr > 50$) for the same reason. For $Fr > 200$, the cavity surface sealed and was pulled beneath the surface before pinching-off resulting in a change in internal cavity pressure and hence the overall cavity dynamics. This, coupled with the distorted cavity shape due to drops impacting the cavity wall made it more difficult to record the precise pinch-off points beyond this limit. In the early surface seal regime of experiments performed at low bond numbers, Aristoff & Bush (2009) denoted the surface seal itself as a pinch-off assigning it a depth of zero. Although they identified the regime for the occurrence of early surface seals and proposed a preliminary theoretical model for splash curtain dynamics coupled with their cavity model, the subsequent deep closures were disregarded.

Gilbarg & Anderson (1948) investigated cavity formation at reduced atmospheric pressures to result in a decreased Bernoulli pressure ($1/2\rho_A V_0^2$) acting on the splash sheet. The result of delaying the surface seal was a relative overpressure in the cavity itself, leading to delayed deep closure (i.e. cavity pinch-off) times. Prior to surface seal, the reduced external pressure was predicted to have little effect on

https://doi.org/10.1017/jfm.2014.35 Published online by Cambridge University Press

cavity formation due to a small influence in the corresponding governing equations. A few studies have also investigated cavity formation at very high impact speeds above 350 m s^{-1} (Metzger 1981) and 400 m s^{-1} (Lee, Longoria & Wilson 1997), respectively, with the objective of predicting cavity dynamics for early surface seal cases. In these conditions, air flowing from the free surface into the cavity at speeds of Mach 1 causes a choked flow which delays surface seal and encourages early pinch-off.

The inability of these studies, using numerical and indirect experimental techniques, to provide precise measurements for cavity dynamics in the early surface seal regime ($Fr > 100$) has motivated this work to develop a simple experimental set-up which prohibits the surface seal phenomenon at standard laboratory conditions (atmospheric pressure, $P_a = 101$ kPa) allowing the study of the ensuing undisturbed cavity dynamics. Although real impacts are accompanied by surface seal and artificially removing them alters the naturally occurring impact cavity's dynamics in comparison, obtaining smooth cavities in an unexplored Froude number regime would test the validity of previously deduced scalings for the reduced pinch-off position (H_p/H) and pinch-off time (τ) in the extended parameter space, mainly for idealized configurations. It would also help to further understand the cylindrical collapse of a cavity and observe other phenomenon previously unseen.

For the purpose of removing surface seals, carefully positioned hollow conical-shaped plastic funnels were used to barricade and direct the surface splash radially outwards to obtain extremely clear cavities with no interference from the incoming surface-seal splash droplets. Figure 1 presents a comparison of two sphere impacts at $V_0 = 8.4$ m s^{-1}; first where the impact was 'unguarded' as in all previous experimental studies, leading to surface seal; the second where the surface seal was prohibited using the splash-guard. See also supplementary movie 1 available at available at http://dx.doi.org/10.1017/jfm.2014.035. The difference is dramatic and allows us to clearly measure the pinch-off depth and time, which was previously not possible. This resulted in accurate measurements for a more extended range of Froude numbers in comparison with Duclaux *et al.* (2007).

In addition to the quest for data in this extended parameter space, we note that no studies have investigated the effect of geometrical confinement on cavities produced by projectile impacts onto liquids. A few studies (Von Kann *et al.* 2010; Royer *et al.* 2008) have explored this subject using sand as the impact medium. This phenomenon again is of importance to several military, industrial, biological and sports applications including the entry of ballistic missiles to a confined liquid spaces, slamming of boats and seaplane landings in slim canals, dip-coating operations in small fluid containers, creatures walking on confined water spaces and drag on swimmers and rowing oars in narrow channels. In light of these applications, this study also investigates confinement effects on the cavities produced by impact of hydrophobic spheres. To this end, the cross-sectional area of the impact tank was systematically decreased in conjunction with the surface seal prevention mechanism which lead to the formation of sequential multiple pinch-offs, for the experimental range of Froude numbers investigated. This paper is thus organized as follows. In the next section, we describe our experimental set-up and protocols. In § 3 we describe the qualitative features of surface seal elimination. In § 4 we first quantify the pinch-off depth and times for the unbounded case, then proceed to examine the influence of geometrical confinement and the observations of surface waves, multiple pinch-offs and acoustic ripples. In § 5, we conclude our experimental observations by presenting asymmetric jet formations due to kinked pinch-offs.

https://doi.org/10.1017/jfm.2014.35 Published online by Cambridge University Press

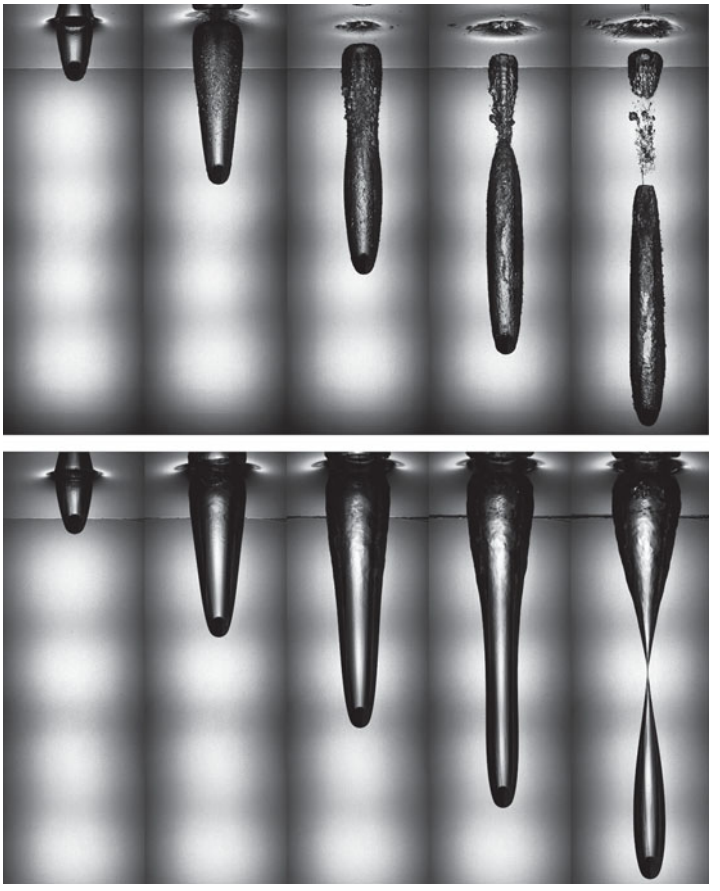


FIGURE 1. Sequence of images showing the cavity formation by impact of a hydrophobic 10 mm radius sphere in a 50×50 cm^2 cross-sectional area tank ($D_{tank} = 50$) at 8.4 m s^{-1} for (*a*) free impact (surface seal) and (*b*) guarded impact (non-surface seal). For both series the first image shown is taken at 7 ms after impact and subsequent images taken at 14 ms intervals. See also supplementary movie 1. Here $\epsilon = 0.04$, $Fr = 720$, $We = 9800$, $Bo = 13.6$ and $C_n = 2.8$.

2. Experimental set-up and parameter space

A schematic representation of the experimental set-up is shown in figure 2. For the impacting bodies, we use steel spheres which were hydrophobized using a commercially available agent, Glaco 'Mirror Coat zero' (Soft99 Corp. Co., Ltd, Japan). The coating contains nanoparticles and organic reagent, resulting in a water contact angle of about 160° (Vakarelski *et al.* 2012). The spheres were attached to an electromagnetic release system positioned directly above the centre of the tank. The tanks were fabricated from Perspex and filled with de-ionized water ($\mu = 1$ cP, $\rho = 996$ kg m^{-3} and $\sigma = 72.1$ mN m^{-1}). For selected experimental conditions, we also used perfluorohexane, C_6F_{14} ($\mu = 1.1$ cP, $\rho = 1710$ kg m^{-3} and $\sigma = 11.9$ mN m^{-1}) as the target liquid.

The mechanism employed to eliminate the surface seal was a plastic hollow cone, which was attached to the edges of the tank using support wires. The cone was positioned in the line of the sphere trajectory. The distance between the base of the

https://doi.org/10.1017/jfm.2014.35 Published online by Cambridge University Press

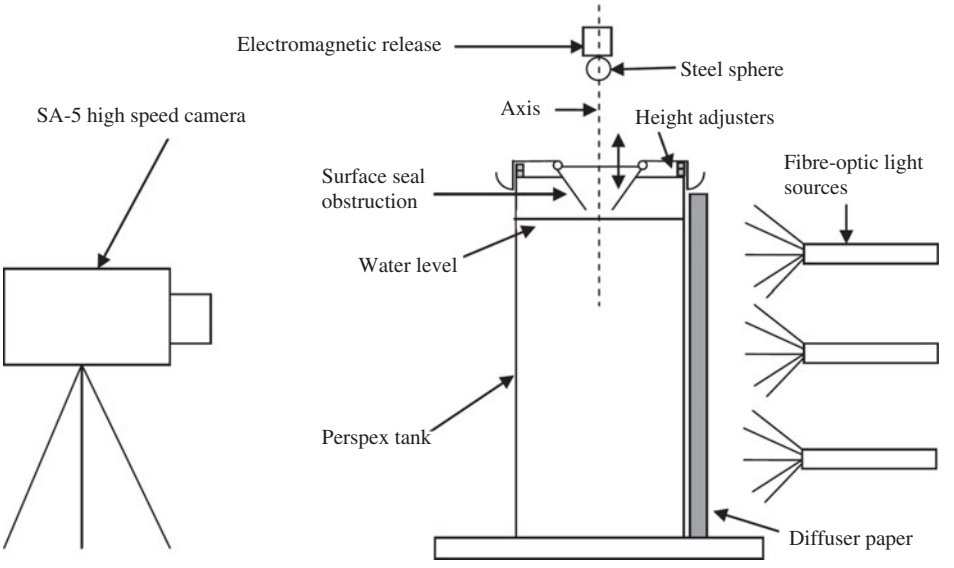


FIGURE 2. Schematic of the experimental set-up used.

cone and the water level was varied depending on the ejecta sheet evolution rate, in turn related to sphere impact speed and sphere size. All of the cones had a thickness of 2 mm, an upper diameter of 100 mm and a 60° angle of inclination. In contrast, the lower diameter was dependent on the sphere diameter allowing for a 5 mm radial clearance for the sphere to pass through.

Upon switching the electromagnet off, the spheres fell freely under gravitational acceleration and passed through the cone hole before impacting the liquid surface at $t = 0$ s with impact speed $V_0 \approx \sqrt{2gh_r}$, where h_r is the release height of the sphere. The cavity formed in the wake of the sphere was made visible using back-illumination dispersed light via a diffuser screen, emanated from four Sumita (350 W) metal halide light sources placed behind the tank. Videos at 15 000 f.p.s. were recorded using a monochrome high-speed camera (Photron Fastcam SA-5) thus rendering silhouette images, which were saved to a storage medium for subsequent examination. The recording duration was long enough for manual triggering. The camera was equipped with either a Nikon 20, 55 or 105 mm lens based on the field-of-view needed. Plastic sheets were attached to the upper edges of the tank in order to contain the ejecta sheet splatter directed radially outwards by the cones. This aided in maintaining a consistent water level and prevent splashing inside the experimental area. The tank water temperature was measured to be the same as the room temperature of 22°C. The time between consecutive trials was at least 10 minutes to ensure impact onto a quiescent pool.

Experiments using particle image velocimetry (PIV) techniques were also performed. In this case, 20–50 μm diameter PIV fluorescent particles ($\rho_p = 0.98$–1.02 g cm^{-3}) were added to water in the smallest tank with $D_{tank} = 8$ cm. After the addition of particles and stirring to ensure a uniform seeding density, the tank was left for several minutes to render a truly quiescent pool. Fluorescence was achieved in a two-dimensional plane using a 0.5 mm thick laser sheet aligned vertically, passing through the centre of the tank. The laser itself (Stellar-Pro ML/150, Modu-Laser) was a continuous wave laser comprising multiple wavelengths from 457–514 nm,

https://doi.org/10.1017/jfm.2014.35 Published online by Cambridge University Press

Parameter	Symbol	Range	Units
Sphere diameter	D_0	15–25	mm
Impact speed	V_0	1.5–8.4	m s^{-1}
Tank diameter	D_{tank}	8–50	cm
Diameter ratio	ϵ	0.03–0.31	–
Froude number	Fr	18–960	–
Bond number	Bo	7.9–21.9	–
Weber number	We	237–12623	–
Cavitation number	C_n	> 2.8	–

TABLE 1. Summary of physical parameters and non-dimensional numbers observed in this study.

whilst the particle fluorescence was isolated using a 527 nm band pass filter on the camera lens. Images were recorded at 7000 f.p.s. using a single camera, thus rendering a pseudo-planar high-speed PIV technique. The captured images were then analysed using a sequential-frame cross-correlation in MATLAB or DaVis 7.2 software (LaVision GmbH).

2.1. *Parameter space*

Spheres of three different diameters $D_0 = 15$, 20 and 25 mm, density $\rho_s = 7800$ kg m^{-3} and roughness $R_a = 0.06$ μm were used. The hydrophobic coating induced additional roughness features with typical submicrometre (∼500 nm) peak-to-trough heights (Marston *et al.* 2012*b*; Vakarelski *et al.* 2012). Each sphere collided with free surfaces in 80 cm deep tanks having five different square cross-sectional areas: 50×50, 40×40, 20×20, 15×15 and 8×8 cm^2. Although cylindrical tanks with circular cross-section would be preferable as they would not influence the axisymmetry of cavity dynamics when wall effects become prominent, they introduce unacceptable optical distortions restricting us to the use of square cross-sectional area tanks. For convenience, hereafter, we refer to the tank size by the minimum diameters, $D_{tank} = 50$, 40, 20, 15 and 8, and the sphere-to-tank diameter ratio is defined as $\epsilon = D_0/D_{tank}$. (Note the actual distance from the sphere edge to the tank wall varies from $(D_t - D_0)/2$ to $(\sqrt{2}(D_t - D_0))/2$.) The impact velocity V_0 ranged from 1.49 to 8.40 m s^{-1}. Non-dimensional parameters relevant to these impacts include the Froude number, Weber number and Bond number which varied in the range 18–960, 237–12 623 and 7.88–21.90, respectively. In addition, we note the cavitation number $C_n = (P - P_v)/(1/2\rho_l V_0^2) \geqslant 2.8$, implying that the creation of flow-induced cavitation bubbles can be neglected. The dimensional and non-dimensional parameters with corresponding ranges are summarized in table 1.

3. Qualitative effect of eliminating surface seal

Figure 3 presents pinch-off images (i.e. the image taken just prior to pinch-off) of cavities obtained by the impact of a $D_0 = 20$ mm superhydrophobic sphere in a tank measuring 50 cm × 50 cm × 80 cm for increasing impact speeds with (*a*) and without (*b*) surface seals (see the caption for details). From the snapshots taken for impacts with surface seal, it can be readily observed that the cavity pinch-off is only well-defined for low impact speeds ($V_0 \leqslant 3$ m s^{-1}). Beyond this, the surface seal induces

https://doi.org/10.1017/jfm.2014.35 Published online by Cambridge University Press

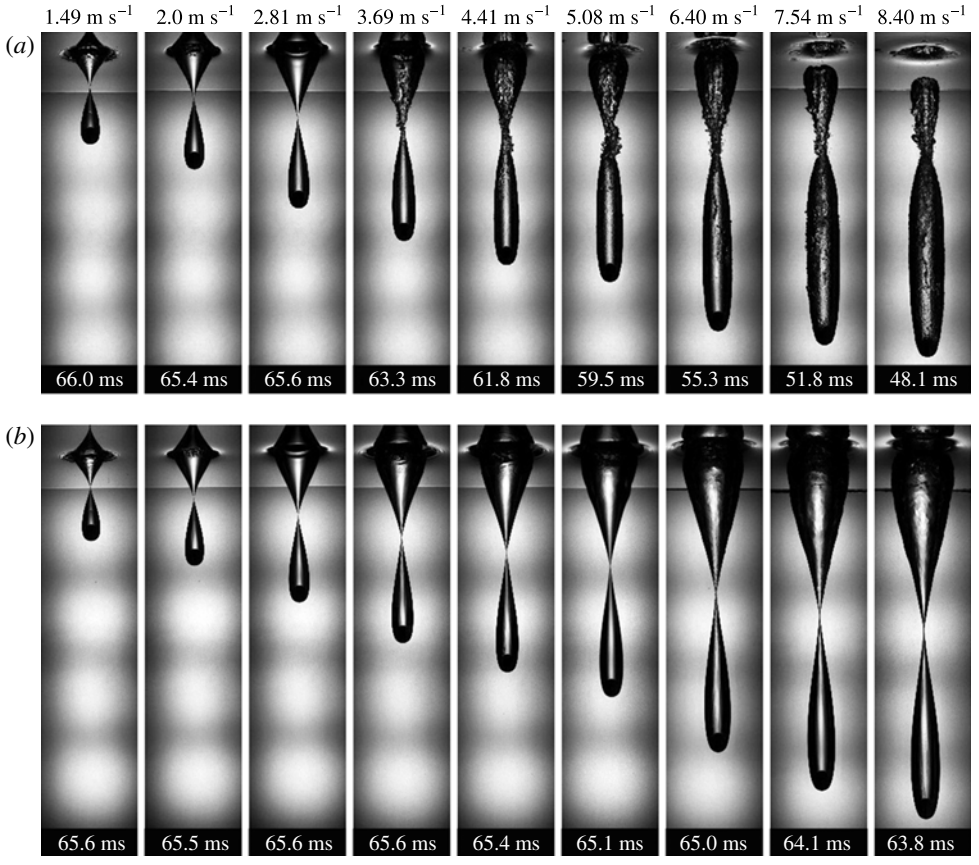


FIGURE 3. Pinch-off images of (*a*) free and (*b*) guarded impact cavities produced by the impact of a $D_0 = 20$ mm hydrophobic sphere with chronological impact speeds of (from left to right) $V_0 = 1.49, 2.0, 2.81, 3.69, 4.41, 5.08, 6.40, 7.54$ and 8.40 m s^{-1}. Here $D_{tank} = 50$ was used to minimize wall effects. The time from impact is stated at the bottom of each image. All images in (*b*) are taken just before the pinch-off. Here $Fr = 22 - 720$ and $\epsilon = 0.04$.

a fine spray of droplets into the cavity, which destroys the smooth appearance and renders the pinch-off depth difficult to measure precisely. In stark contrast, when we employ the cone splash-guard, the surface seal is eliminated and the cavity pinch-off can be accurately located in both space and time for all impact speeds. This is further highlighted by the zoomed views of the necking just prior to pinch-off in figure 4. The pinch-off depths are larger compared with corresponding cases where the cavity experiences the early surface seal phenomenon. The other major discrepancy noted is that the cavity becomes engulfed beneath the surface for impact speeds greater than 6.40 m s^{-1}, which was not observed for the 'guarded' impact cases since the cavity is bounded at the free surface by the bottom of the cone. As such, we can extend the measurements of cavity pinch-off into a higher regime of impact Froude numbers than reported previously, which will enable us to provide a more thorough examination of the scaling given by Duclaux *et al.* (2007).

In figure 5, we present digitized cavity shapes from figure 3(*b*), for the guarded impacts, which have been scaled with respect to the corresponding lengthscale tV_0

https://doi.org/10.1017/jfm.2014.35 Published online by Cambridge University Press

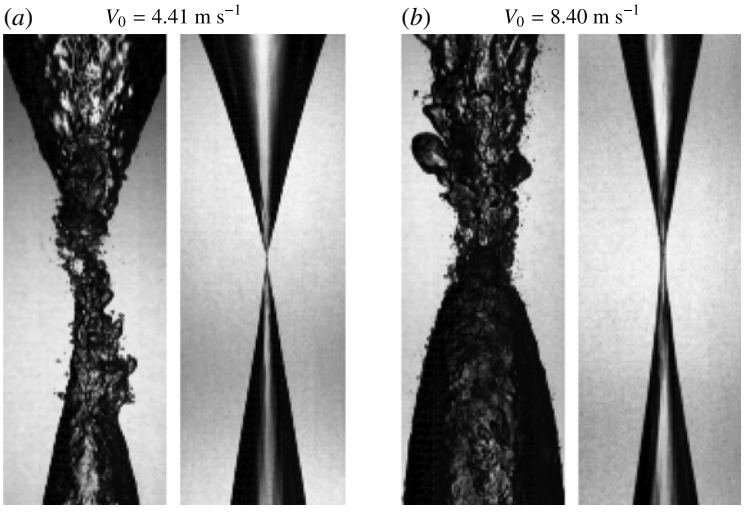


FIGURE 4. Zoomed views of the necking region, just prior to pinch-off for both free (left) and guarded (right) impacts (where the surface seal is eliminated). $D_0 = 20$ mm, $D_{tank} = 50$ cm, $Fr = 198$, $\epsilon = 0.04$ and (*a*) $V_0 = 4.41$ m s^{-1} and (*b*) $V_0 = 8.4$ m s^{-1}.

for each case. These shapes were determined using a customized edge-detection routine in MatLab, with the origin $(x, z) = (0, 0)$ corresponding to the location of the pinch-off point. We can clearly see that under these scalings, the relative size of the cavity decreases to form a more streamlined configuration, and appears to be approaching a self-similar shape for $V_0 \geqslant 5.08$ m s^{-1}, as the shapes for this regime collapse reasonably well onto each other. This corresponds to impact Froude numbers, $Fr \geqslant 263$ and impact Reynolds numbers, $Re = \rho D_0 V_0/\mu \geqslant 1 \times 10^5$. In addition, we calculate the scaled bubble volume and find it to exhibit a power-law dependence on the Froude number as $V_{bub}/R_0^3 \propto Fr^{\lambda}$, with $\lambda = 0.74$. This is in good agreement with the result of $\lambda = 0.78$ by Bergmann *et al.* (2009) for disc impacts, indicating the universality of the entrained air volume in water entry problems.

4. Results and discussion

4.1. *Surface seal removal for negligible wall effects*

In figure 6, we plot data for the scaled pinch-off location H_p/H and pinch-off time τ as a function of the Froude number for different sphere sizes ($R_0 = 7.5$, 10 and 12.5 mm) for negligible wall effects with $D_{tank} = 50$ cm. Here H_p is the depth of the pinch-off point below the initial free surface and H is the depth of the centre of the sphere at the time of pinch-off. Experimental results obtained by Duclaux *et al.* (2007) were assigned a constant value of $H_p/H = 0.45$ close to a value of 1/2 obtained theoretically. Contrary to this, the results shown in figure 6(*a*) reveal qualitatively different trends for H_p/H with increasing Froude number for both surface seal and non-surface seal impacts.

For Froude number values $18.1 \leqslant Fr \leqslant 64.5$, H_p/H values for all three sphere sizes in the guarded and unguarded case increased gradually from 0.39 to 0.43. For this range of Froude numbers, the surface seal occurs after pinch-off for all three spheres, rendering the data sets for free and guarded impacts indistinguishable. For $Fr > 64.5$, 80.6 and 107.5, corresponding to sphere radii $R_0 = 12.5$, 10 and 7.5 mm,

https://doi.org/10.1017/jfm.2014.35 Published online by Cambridge University Press

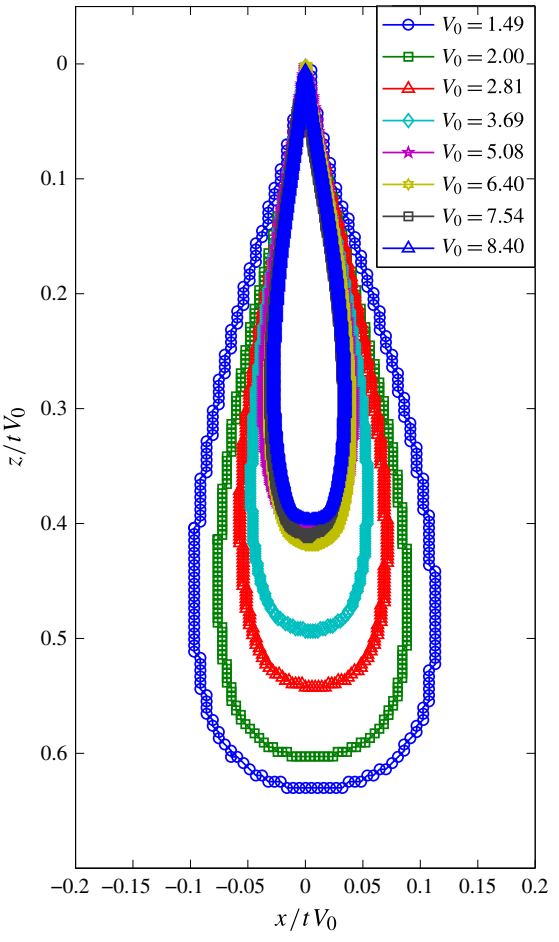


FIGURE 5. (Colour online) Cavity shapes from the guarded impacts without surface seal, shown in figure 3(*b*) and scaled with respect to τV_0. The origin, $(x, z) = (0, 0)$, corresponds to the location of the pinch-off point. The legend indicates impact speeds in m s. Here $Fr = 22$–720 and $\epsilon = 0.04$. Note the collapse of the profiles for $V_0 \geqslant 5.08$ m s^{-1} with corresponding impact Reynolds numbers, $Re = \rho D_0 V_0/\mu \geqslant 1 \times 10^5$.

respectively, the surface seals prior to pinch-off, if no guard is used. This restricts the internal pressure in the cavity (as no more air can enter), limiting the pinch-off depth and hence decreasing the H_p/H values to a minimum of 0.32. Here, the measurement of the absolute value of H_p is accurate only to within ± 1 cm, with notable scatter depicted by the sizable error bars. In contrast, when the surface seal is eliminated, the scaled pinch-off depth gradually increases throughout the entire range of Froude numbers studied as air can flow into the cavity, maintaining the internal pressure at atmospheric pressure. The values of H_p/H at the maximum Froude number obtained were 0.511, 0.489 and 0.461 for sphere sizes of $R_0 = 7.5$, 10 and 12.5 mm, respectively, showing reasonable agreement with the theoretical prediction made by Duclaux *et al.* (2007) where $H_p/H = 1/2$. We note however that this theoretical value is obtained only for spheres which have not decelerated significantly during their fall. For the non-decelerating case the depth of the sphere at pinch-off time can be given

https://doi.org/10.1017/jfm.2014.35 Published online by Cambridge University Press

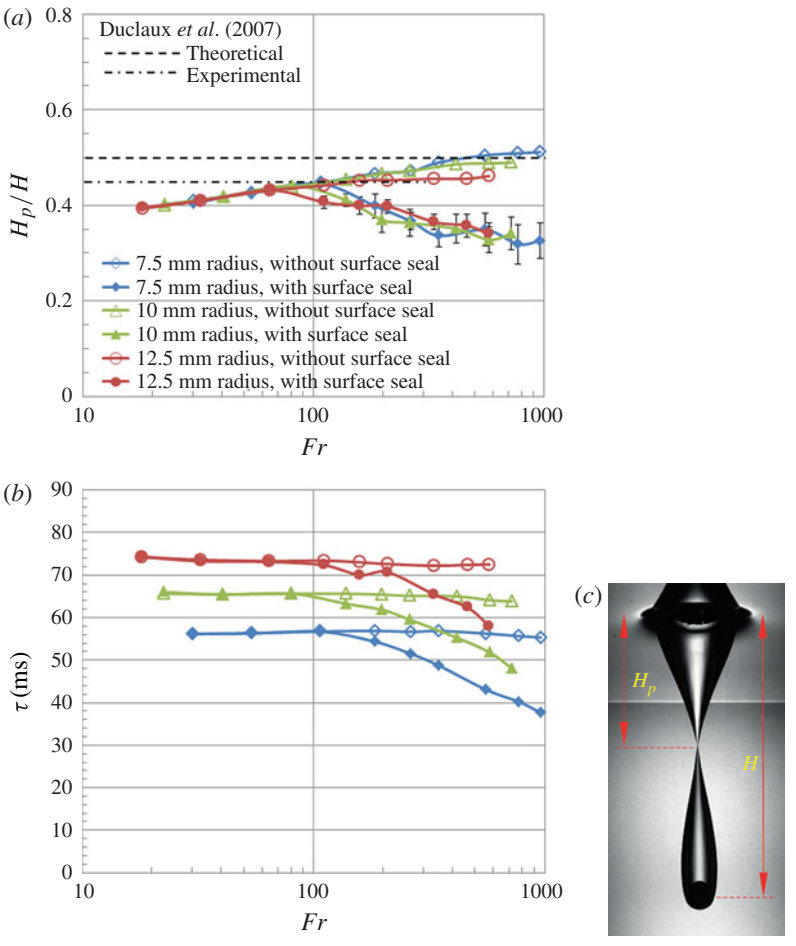


FIGURE 6. (Colour online) (*a*) Scaled pinch-off depth H_p/H and (*b*) pinch-off time τ as a function of the Froude number for both guarded (no surface seal) and free (with surface seal) impacts in a 50×50 cm^2 cross-sectional area tank for different sphere sizes. We note the H_p/H and τ values to decline when the surface seals prior to pinch-off. The variation in H_p/H values in this range is represented by error bars. The image in (*c*) shows graphical definitions of H_p and H.

by $V_0\tau$ leading to a normalized pinch-off position scaling of $H_p/(V_0\tau)$. Calculating the results in this manner for non-surface seal cavities we obtain a steady value of $H_p/(V_0\tau) = 0.4$.

In summary, whilst the free (i.e. with surface seal) impacts exhibit marked scatter and general decline in H_p/H, for the guarded impacts we observe H_p/H values to increase gradually from 0.4 up to 0.5 as the Froude number increases across two orders of magnitude. For non-decelerating spheres a steady value of $H_p/(V_0\tau) = 0.4$ is obtained. These results differ slightly from those by Duclaux *et al.* (2007) who concluded with a constant experimental value of $H_p/H = 0.4$ and a theoretical value of 0.5 for non-decelerating spheres.

In figure 6(*b*), we observe the pinch-off times to be clearly independent of the sphere impact velocity, determined solely by the sphere radii for $Fr < 100$ in

https://doi.org/10.1017/jfm.2014.35 Published online by Cambridge University Press

both surface seal and non-surface seal cases. This trend is found to persist if the Froude number is increased with guarded surface seals leading to constant pinch-off times of 56.4, 65.6 and 73.7 ms for spheres of radii $R_0 = 7.5$, 10 and 12.5 mm, respectively. These agree extremely well with the cavity pinch-off times for hydrophobic sphere impacts determined by Duclaux *et al.* (2007) as 56.95, 65.77 and 73.53 ms corresponding to 7.5, 10 and 12.5 mm radius spheres, from their empirical equation $\tau = 2.06\sqrt{(R_0/g)}$. For the free impacts, however, there is a marked decline in pinch-off times for Froude numbers $Fr > 100$. These pinch-off times could not be measured with the same degree of accuracy as those obtained for the guarded impacts. Nevertheless, a maximum reduction of 31.09, 26.14 and 18.34 % in pinch-off times was noted for spheres sizes of $R_0 = 7.5$, 10 and 12.5 mm, at Froude numbers $Fr = 960$, 720.6 and 576.5, respectively. The reduction in pinch-off times is again due to the fact that the surface seal occurs earlier as the impact speed increases, with similar reductions in surface seal time noted by Gilbarg & Anderson (1948).

4.2. *Influence of wall effects on cavity shape*

Wall effects for falling spheres, normally summarized by a *wall factor*, f_w, itself a function of both the sphere-to-tank diameter ratio, $\epsilon = D_0/D_{tank}$, and the Reynolds number, typically become prominent when the ratio $\epsilon > 0.05$ (e.g. Di Felice 1996). Hence, experiments performed with $D_{tank} = 50$ are expected to exhibit negligible wall effects but as the tank sizes were systematically reduced further, the increasing wall effects demonstrated a strong influence on the cavity shape, pinch-off depth and time with increase in sphere impact speed and size. All results presented hereafter are for cavities observed for the guarded impacts.

Figure 7 shows images captured just prior to the first pinch-off of a guarded impact cavity from a 10 mm radius sphere at 8.4 m s^{-1} in different tank diameters from $D_{tank} = 50$ to 15 cm. We immediately observe that wall effects result in delayed cavity pinch-off, noted by the pinch-off times below the images, and the formation of prominent wave-like structures or undulations along the cavity interface, the wavelengths of which appear to decrease as the severity of the geometrical constraint increases. We also note a decreasing pinch-off depth as $D_{tank} : 50 \rightarrow 20$. However, upon further reduction to $D_{tank} = 15$, this trend reverses to result in a significantly longer pinch-off depth with the presence of surface undulations above and below the pinch-off point.

For cavities produced in the presence of even larger wall effects ($D_{tank} = 8$, $\epsilon = 0.19$), we present a series of images taken just prior to pinch-off in figure 8 for a large range of impact speeds (see the caption). We clearly note the increase in wavelengths of the surface undulations as the impact speed increases and decrease with increase in depth. Note that the undulation closest to the sphere has a consistent wavelength of $\lambda \approx 4.5$ cm. We also observe how surface undulations are gradually induced above and below the first pinch-off point. The crests of these undulations are found to be favourable points for cavity closure which can lead to the formation of multiple pinch-offs (see § 4.4). For $V_0 \leqslant 5.08$ m s^{-1}, $V_0 = 6.40$ m s^{-1} and $V_0 \geqslant 7.54$ m s^{-1}, the first pinch-off in time is noted to occur at the first, second and third crest from the surface, respectively. We present all data in this study based on a time-based numbering system where the first pinch-off is the earliest to occur in time.

Although Worthington (1908) and Mallock (1918) mentioned about ripples on entrained cavities attached to fast moving objects after they have impacted a free liquid surface, only two recent studies (Grumstrup, Keller & Belmonte 2007; Gekle

https://doi.org/10.1017/jfm.2014.35 Published online by Cambridge University Press

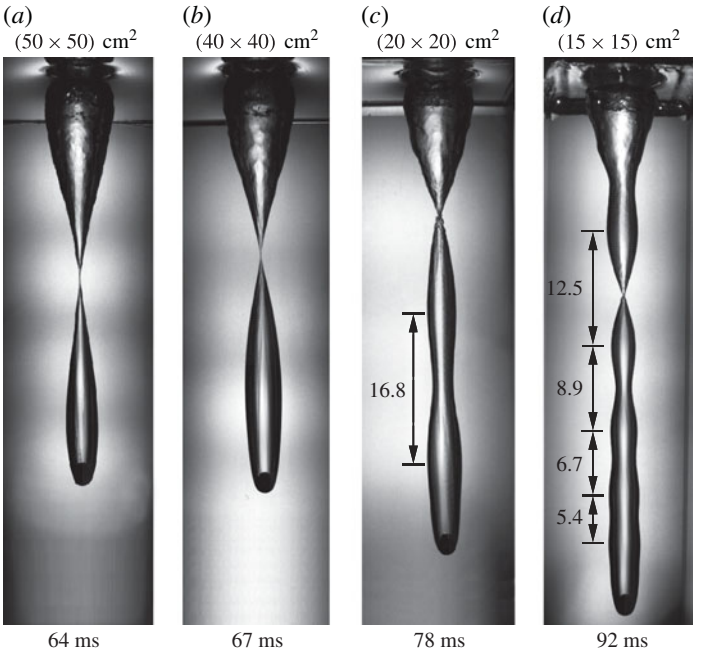


FIGURE 7. Images taken just prior to the first pinch-off of guarded surface seal cavities produced by impacting a 10 mm radius sphere at 8.4 m s^{-1} in different tank sizes $D_{tank} = 50,\ 40,\ 20$ and 15 (left to right). The time from impact for each image has been marked and obvious surface undulation wavelengths have been shown in centimetres. Here $Fr = 720,\ \epsilon = D_0/D_{tank} = 0.04,\ 0.05,\ 0.1$ and 0.133.

et al. 2008) have explored this phenomenon in further detail. For long entrained cavities produced by impact of rough steel spheres of diameter ($D_0 = 0.5$ in.) at $V_0 = 1$–5 m s^{-1}, Grumstrup *et al.* (2007) reported that ripples were observed only after the primary cavity pinch-off. The rippling wavelength λ was found to be approximately equal to the diameter of steel spheres used, i.e. $\lambda = O(D_0)$. They suggested the ripples to be acoustic in origin and attributed them to resonant volume oscillations of the cavity, instigated by the pressure perturbation of the pinch-off event. In addition, it was shown that the product of ripple wavelength λ and the acoustic frequency f was equal to speed of the projectile V_0 ($\lambda f = V_0$), which suggested the projectile to be an acoustic source which affected the fluid only locally, as it passed by. These cavity ripples were shown to be independent of surface tension as they obtained similar ripple wavelengths for experiments performed in ethanol and water. Note that the sphere-to-tank ratio in their study $\epsilon \leqslant 0.1$, so that in accordance with our observations in figures 7 and 8, one would not have expected surface undulations in the experimental configuration in Grumstrup *et al.* (2007).

In a different experimental configuration, Gekle *et al.* (2008) dragged a smooth cylinder (radius, $R_0 = 20$ mm, and length, $l = 147$ mm) at a constant speed $V_0 =$ 0.5–2.5 m s^{-1} through a water surface and found ripples to appear as soon as the top of the cylinder passed the water surface, rather than at pinch-off. The ripples were determined to be capillary in nature, due to the typical wavelength $\lambda = O$(mm). These, in addition to the hydrostatic pressure led to the occurrence of two distinct regimes in

https://doi.org/10.1017/jfm.2014.35 Published online by Cambridge University Press

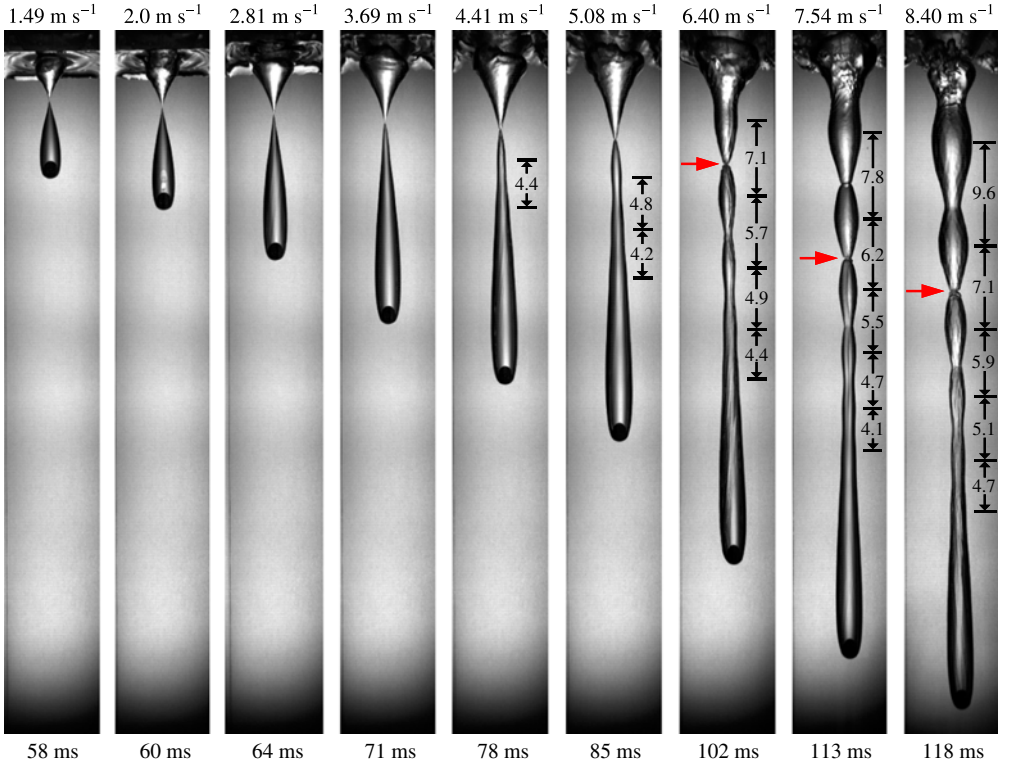


FIGURE 8. (Colour online) Pinch-off images of guarded (no surface seal) impact cavities for a hydrophobic sphere with chronological impact speeds of (from left to right) $V_0 = 1.49$, 2.0, 2.81, 3.69, 4.41, 5.08, 6.40, 7.54 and 8.40 m s^{-1}. Here $D_0 = 15$ mm, $D_{tank} = 8$ cm, $\epsilon = D_0/D_{tank} = 0.19$ and $Fr = 30$–960. The time from impact for each image has been marked and the surface undulation wavelengths have been measured in centimetres. The arrows (shown in red online) indicate the first pinch-off positions for better clarity. See also supplementary movie 2.

the cavity closure depth H_p as a function of Froude number, with a transition region where $Fr \approx 10$–20, hence indicating the non-universality of cavity collapse.

Similar to Gekle *et al.* (2008), figures 7 and 8 reveal the existence of prominent wave-like structures *prior* to cavity pinch-off, however, the wavelengths are found to range between 1 cm $\lesssim \lambda \lesssim$ 15 cm, which would typically correspond to the regime of gravity-capillary waves whereby both the surface tension and gravity (only when acting perpendicular to the free surface) are important. In light of this, we performed experiments in the smallest tank, $D_{tank} = 8$ cm, with perfluorohexane (C_6F_{14}) with a surface tension of $\sigma = 11.9$ mN m^{-1}, to compare with the wavelengths of undulations in water with increasing distance from the free surface level. The results of this are shown in figure 9, where $D_0 = 15$ mm is used with various impact velocities (see the legend). Although these measurements are independent of the time from impact (due to the suspected fixed nature of the undulations), we have recorded them from the cavity shapes at the first pinch-off time. Results obtained by Gekle *et al.* (2008) for capillary waves have also been included in the inset to the figure. From the plot we clearly see wavelengths produced in perfluorohexane to be significantly smaller (approximately half) than corresponding values in water (for $V_0 = 8.4$ m s^{-1}).

https://doi.org/10.1017/jfm.2014.35 Published online by Cambridge University Press

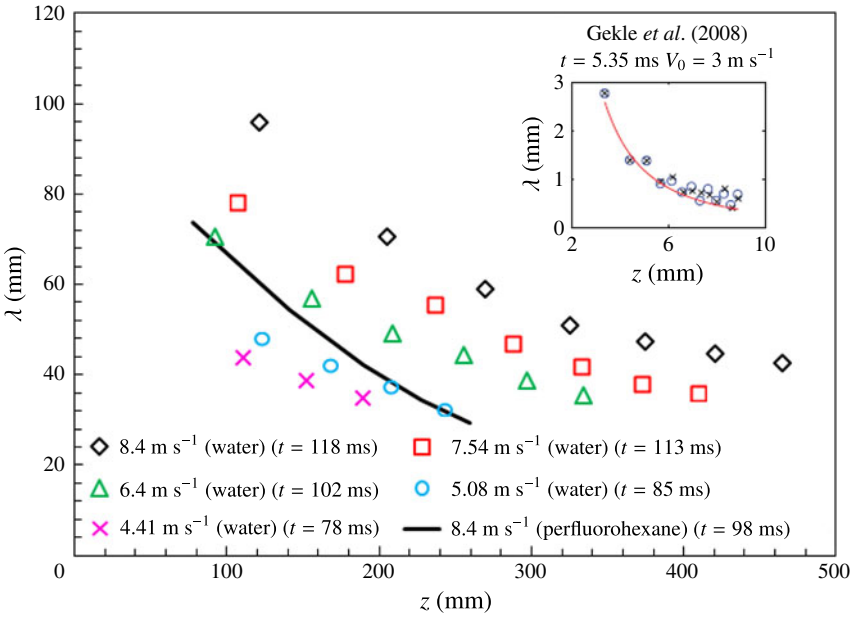


FIGURE 9. (Colour online) Surface undulation wavelengths versus distance from free surface level at the first cavity pinch-off time produced by impact of hydrophobic sphere at various impact speeds with different fluids (see the legend). Here $D_0 = 15$ mm, $D_{tank} = 8$ cm, $\epsilon = 0.19$ and $Fr = 264$–960. The inset shows results obtained by Gekle *et al.* (2008) in water.

Although the density of perfluorohexane (1700 kg m^{-3}) is higher than that of water, which results in only a slightly lower sphere velocity as it falls through the tank, the large decrease in wavelength is substantial enough to suggest that surface tension is important; The fact that surface tension should act to support the lifetime of the cavity interface is consistent with this observation. At a qualitative level, we see that the trend of decreasing wavelength with increasing distance from the initial free surface is common to both the surface undulations observed in our studies and the capillary waves in Gekle *et al.* (2008).

We propose that a potential origin of the wave-like structures observed herein is qualitatively different from the mechanism proposed by Gekle *et al.* (2008), or the acoustic waves observed by Grumstrup *et al.* (2007) and Aristoff & Bush (2009). Rather, due to the wavelength and stationary nature (see § 4.2.1 below), it appears that the surface undulations herein are a confluence of both geometrical confinement, leading to fluid flow parallel to the cavity (see below) and physical attachment of the upper edge of the cavity to the cone.

4.2.1. *Velocity field measured by PIV experiment*

Based on the observations of the progressive undulation formation with increasing geometrical constraints, it is also clear that the fluid motion between the cavity interface and the tank wall must begin to play a significant role in both the undulation formation and the cavity pinch-off location and time. This is intuitive since one would expect the rate of change of momentum in this case to balance the pressure gradient in the governing equation of motion by the inclusion of a vertical component.

https://doi.org/10.1017/jfm.2014.35 Published online by Cambridge University Press

In order to assess the fluid flow in the constrained geometry, and to verify the stationary nature of the undulations, we conducted further experiments employing PIV techniques (see § 2 for details).

For a sphere $D_0 = 15$ mm impacting at 8.4 m s^{-1} in a 8×8 cm^2 cross-sectional area tank, figure 10 shows instantaneous velocity vector fields and figure 11 plots the distribution of (*a*) *u*-radial and (*b*) *w*-vertical velocity components at a depth of 27 cm from the free surface level. This corresponds to the fourth undulation crest (second pinch-off position) from the liquid surface shown in figure 8 for $V_0 = 8.4$ m s^{-1} (located below the arrow).

From these Figures, we observe a significant radial motion towards the tank wall as soon as the sphere passes by (figure 11*a*, 54 ms from impact). The enlarging cavity in the wake then forces the fluid against the tank wall whereby the flow becomes purely unidirectional facing upwards (figure 10, 70 ms from impact). The upward flow is simply demanded by continuity as the growing air cavity forces out the fluid. As the cavity elongates with increasing time and starts to shrink radially, the fluid starts to turn and flow radially inwards (figure 10, 87 ms from impact) and the upward longitudinal motion gradually diminishes until the flow direction reverses (figure 11*b*, 103 ms from impact). At pinch-off (figure 11, 120 ms from impact) near the necking region both the *u*-component and *w*-components rapidly increase inwards and upwards, respectively, while the fluid further away $x > 3$ mm still flows downwards. Immediately after pinch-off (figure 11, 121 ms from impact) near the necking region, the inward facing *u*-component subdues and the *w*-component reverses direction becoming parallel to the fluid flow at $x > 3$ mm flowing downwards with the lower cavity.

We hence find the fluid motion in the vicinity of a surface undulation in the presence of wall effects to be primarily dictated by the time-dependent radial expansion and contraction of the cavity and bounding forces from the tank walls. If the observed undulations were traveling, their crests would be moving downwards towards the base of the tank and the motion of fluid, very near the cavity interface, would have clearly propagated along with the undulation at all times. Since we do not observe these phenomenon in our PIV results, we conclude that the axial surface modulation of the cavity obtained in this study appears to have a stationary nature with respect to the lab frame.

We also observe an irregular or 'kinked' pinch-off in elongated cavities under wall effects. Obvious examples include the cavity pinch-off obtained in figure 10 at 120 ms from impact and that in figure 7 obtained with $D_{tank} = 20$ at 78 ms from impact. These are unlike smooth cavity pinch-offs observed in the absence wall effects. We discuss this phenomenon in detail in § 5.

4.3. *Influence of wall effects on primary pinch-off location and time*

Figure 12 shows data plots for the depth of the primary cavity pinch-off for (*a*) depth versus increasing sphere impact speeds, (*b*) scaled depths versus the Froude number and (*c*) pinch-off times versus the Froude number for various sphere and tank sizes. Results obtained for $D_0 = 20$ and 25 mm at high impact speeds in the smallest tank have been withheld due to cavity distortion arising from dynamical interaction with the splash guard, whilst results for $D_{tank} = 40$ and 50 cm indicate the wall effects to be negligible for $\epsilon < 0.075$.

Although we generally note a decreasing trend in normalized pinch-off depth with increase in wall effects, noted by decreasing H_p for fixed V_0 as $D_{tank} : 50 \rightarrow 8$,

https://doi.org/10.1017/jfm.2014.35 Published online by Cambridge University Press

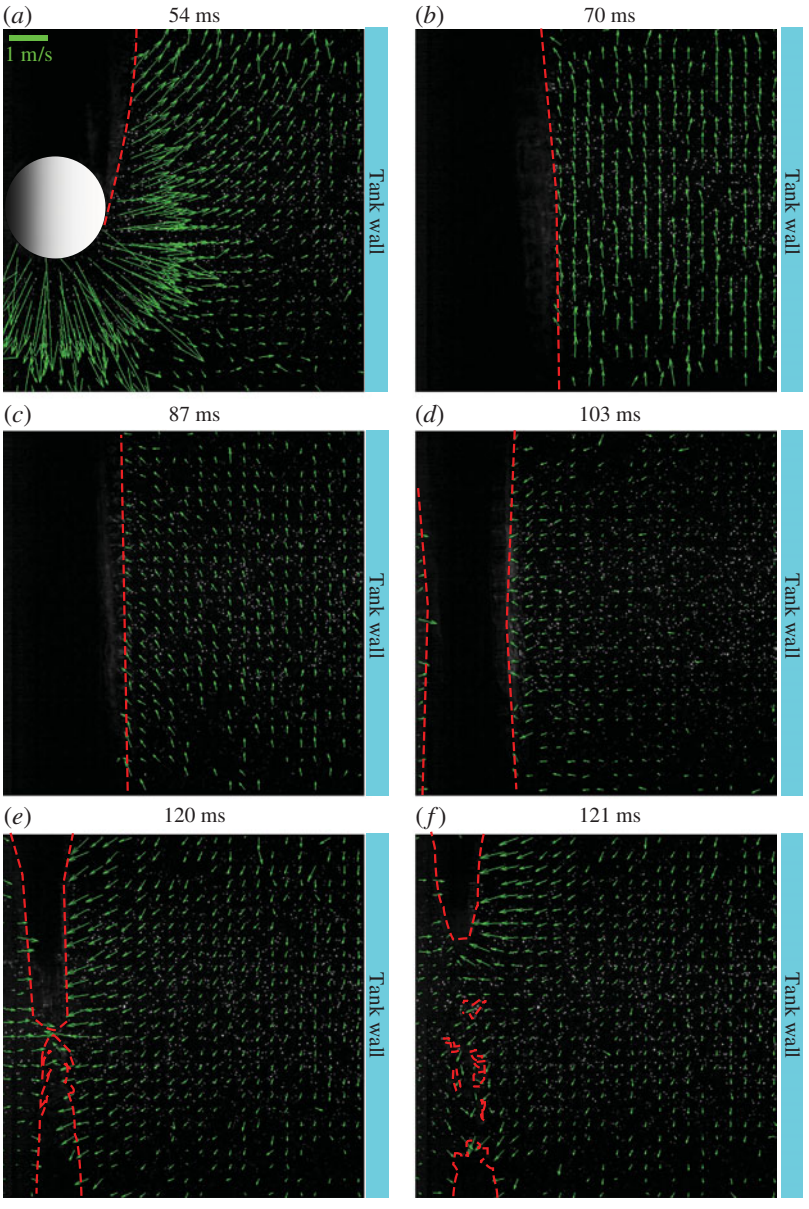


FIGURE 10. (Colour online) Instantaneous velocity fields taken at a depth of 27 cm below the free surface level (fourth undulation crest location from the liquid surface in figure 8 at $V_0 = 8.4$ m s^{-1}) produced by impact of a hydrophobic sphere with water. Here $D_0 = 15$ mm, $D_{tank} = 8$ cm, $V_0 = 8.4$ m s, $Fr = 960$ and $\epsilon = 0.19$. The time from impact has been marked above each image and the dashed line (shown in red online) marks the cavity–water interface. The scale bar at the top left corner shows the vector length representing 1 m s^{-1}.

H_p values obtained for $D_{tank} = 8$ and 15 cm jump and appear to be comparatively much higher than those obtained for $D_{tank} \geqslant 20$ for $V_0 \geqslant 6.40$ m s^{-1}. This behaviour is attributed to the onset of marked surface undulations, some of which appear above

https://doi.org/10.1017/jfm.2014.35 Published online by Cambridge University Press

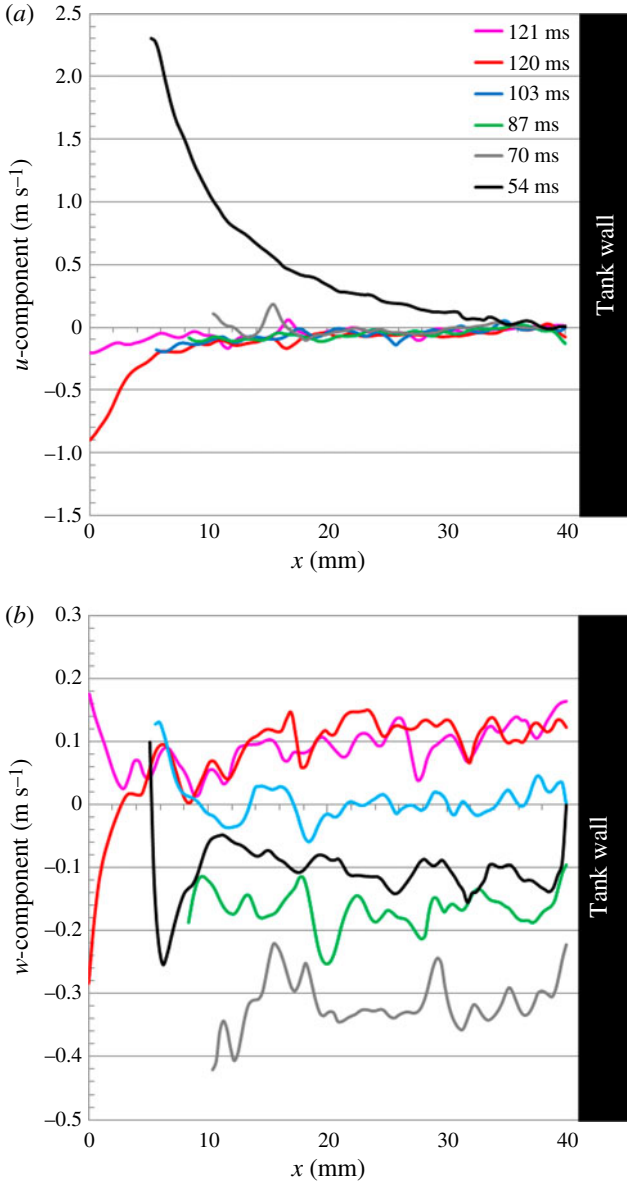


FIGURE 11. (Colour online) Plots of (*a*) the (radial) *u*-component velocity distribution and (*b*) the (vertical) *w*-component velocity distribution versus radial distance from the cavity wall to the tank wall at 27 cm from free surface level (fourth undulation crest location from the liquid surface in figure 8 at $V_0 = 8.4$ m s^{-1}) for corresponding times (see the legend) from impact shown in figure 10. Since the tank has a hydraulic diameter of 80 mm, a radial distance of 40 mm from the pinch-off point marks the tank wall. The pinch-off occurs at 120 ms from impact. Hence, data obtained at 120 ms and 121 ms is shown along the distance from the tank centre (0 mm) to tank wall (40 mm). The positive *u*-component values refer to flow towards the tank wall (east), whilst the positive *w*-component values are away from the free surface level (south).

https://doi.org/10.1017/jfm.2014.35 Published online by Cambridge University Press

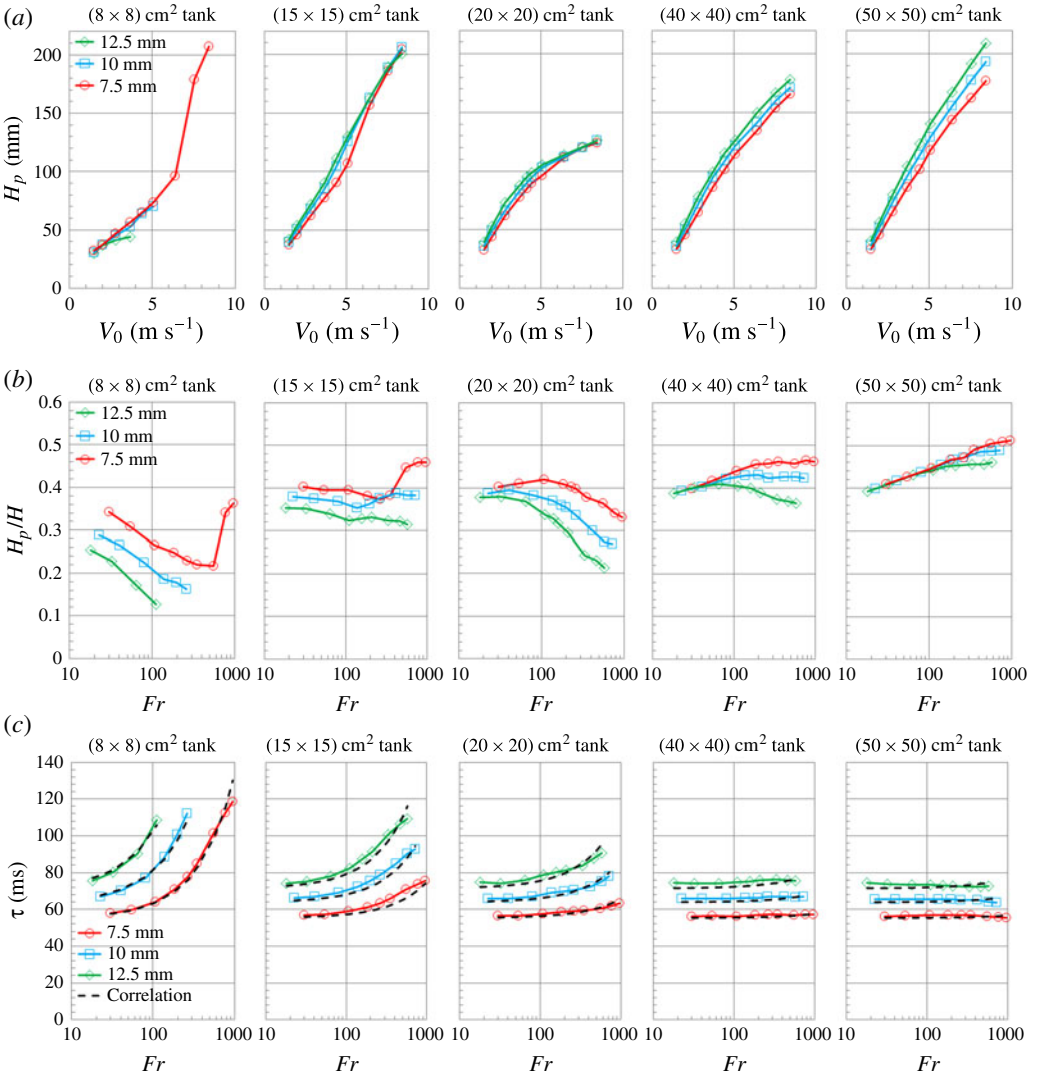


FIGURE 12. (Colour online) The first (*a*) pinch-off depth H_p (mm) versus sphere impact speed V_0 (m s^{-1}), (*b*) scaled pinch-off depth (H_p/H) versus the Froude number and (*c*) pinch-off time τ (ms) versus the Froude number for guarded surface seal cavities produced by impact of various sphere radii in five different cross-sectional area tanks (see the legend).

the first pinch-off point, leading to pinch-off occurring at the second or third wave crests (see figure 8 for the largest impact velocities).

Gekle *et al.* (2008) found two distinct regimes for cavity pinch-off depth in terms of the impact Froude number, separated by a pronounced jump whereby pinch-off depths increased at different rates with increase in impact velocities. In our experiments, however, we initially observe a *decrease* in H_p/H as Fr increases, then a switch to increasing H_p/H values. Clearly, this effect is attributed to different mechanisms: in Gekle *et al.* (2008) due to the onset of capillary ripples, whereas for our experiments,

https://doi.org/10.1017/jfm.2014.35 Published online by Cambridge University Press

due to the pronounced surface undulations arising from geometrical confinement. It would therefore be interesting to observe the cavity dynamics for Gekle's experiment in a confined tank.

In the limit of high Weber number, Reynolds number and 'moderate' Froude number: ($We \gg 1$, $Re \gg 1$, $10 < Fr < 330$) Duclaux *et al.* (2007) showed theoretically that the pinch-off time, τ, in the presence of no wall effects would scale linearly with $\sqrt{R_0/g}$ and hence be independent of impact velocity. Using a best fit to experimental data they found $\tau = 2.06\sqrt{R_0/g}$ which agreed well with our results in the absence of wall effects, shown in figure 6(*b*). When the wall effects are present the pinch-off times shown in figure 12(*c*) are observed to increase monotonically with both increasing sphere size (as expected) *and* impact velocity (unexpected). The degree of the dependence on impact velocity itself is a function of the tank size, that is to say $\tau = f(V_0, \epsilon)$. If we seek a modified form of the fit to $\tau \propto \sqrt{R_0/g}$, we find that the inclusion of both Fr and ϵ in the proportionality constant as $k \approx 2 + (\epsilon^2/10)Fr$ provides a good empirical fit to the full range of our data. The sphere depth at first pinch-off time can then be approximated simply as $H \approx V_0\tau$.

4.4. *Multiple and acoustic pinch-offs*

Having shown that the formation of large wavelength cavity undulations in the presence of wall effects can result in multiple cavity pinch-offs, we now study this phenomenon in further detail and also investigate the formation of a qualitatively different type of surface rippling that appears only after the primary cavity pinch-off.

Figure 13 presents sequences of images showing the formation of multiple pinch-offs for guarded impact cavities produced in restricted geometries with (*a*) $\epsilon = 0.19$, $Fr = 557$ and (*b*) $\epsilon = 0.13$, $Fr = 418$ (see the caption for dimensional parameters). In both series of events shown we observe the onset of a new wave formation emanating from the sphere surface as soon as the first cavity pinch-off occurs. This new wave is manifested by distinct ripples as the sphere travels downwards. These observations are very similar to those reported by Grumstrup *et al.* (2007) who noted ripples emanating from the sphere that coincided with occurrence of cavity closure (pinch-off) and suggested them to be an acoustic phenomenon, initiated by the pressure perturbation of the deep seal. These similarities imply that the ripples we observe originating from the sphere after the primary pinch-off are also acoustic in origin.

The dashed lines in figure 13(*a,b*) indicate the depth of a different kind of pinch-off, where the pinch-off itself occurs at the depth of the sphere when the primary pinch-off occurs, i.e. H. This is the position of the crest of an acoustic ripple and since acoustic ripples originate from the pressure perturbation of the first pinch-off, we thus refer to this new pinch-off as the 'acoustic' pinch-off. In accordance with Grumstrup *et al.* (2007) all subsequent shedding is referred to as 'cavity shedding'. For example, the 'acoustic pinch-off' in figure 13(*a*) is the eighth pinch-off with respect to time from impact.

Grumstrup *et al.* (2007) found the acoustic ripples to have wavelengths of the order of the sphere diameter and verified their acoustic origin by the fact that the product of the ripple wavelength λ_a and the acoustic frequency f was equal to the projectile speed at cavity pinch-off U_0, that is $f\lambda_a = U_0$. Here, we also find that $\lambda_a = O(D_0)$, with a slight variation from $2D_0/3 - 5D_0/3$ possibly due to the multiple previous pinch-offs each causing a distinct pressure perturbation. This is supported by observing the number of ripples marked in figure 13(*a,b*) respectively. For example, in figure 13(*a*), there are eight pinch-offs prior to the image shown at 152 ms, with nine notable

https://doi.org/10.1017/jfm.2014.35 Published online by Cambridge University Press

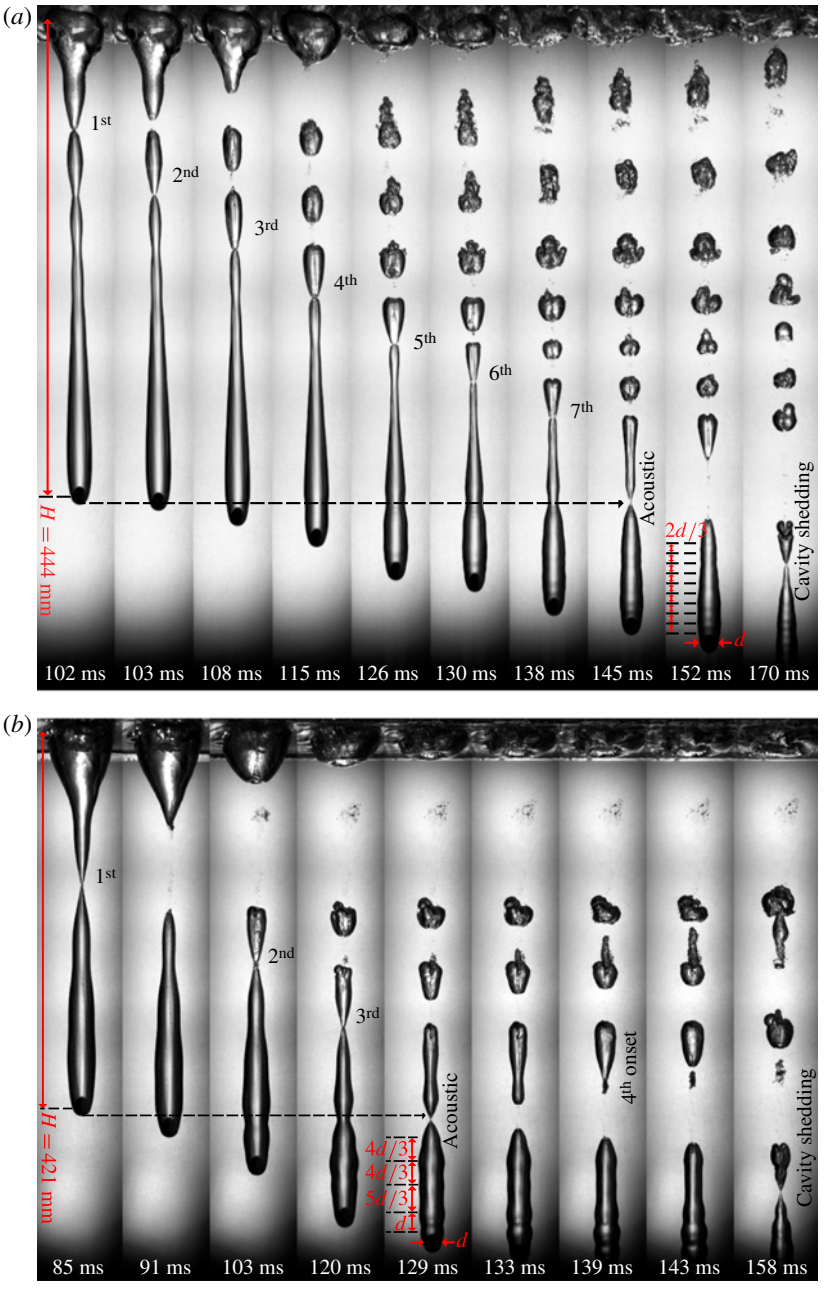


FIGURE 13. (Colour online) Sequence of images showing multiple cavity pinch-offs and acoustic pinch-offs produced by guarded impacts of (*a*) $D_0 = 15$ mm and (*b*) $D_0 = 20$ mm into tanks with (*a*) $D_{tank} = 8$ cm and (*b*) $D_{tank} = 15$ cm, both with impact speed $V_0 = 6.4$ m s^{-1}. Here (*a*) $\epsilon = 0.19$, $Fr = 557$ and (*b*) $\epsilon = 0.13$, $Fr = 418$. The first acoustic pinch-off has been labelled 'acoustic' and subsequent pinch-offs as 'cavity shedding' in each figure. Time from impact has been shown at the bottom of each image. The sphere depth at the primary cavity pinch-off has been marked and the first acoustic pinch-off is noted to occur at this depth at $t = 145$ ms and 129 ms from impact in (*a*) and (*b*), respectively.

https://doi.org/10.1017/jfm.2014.35 Published online by Cambridge University Press

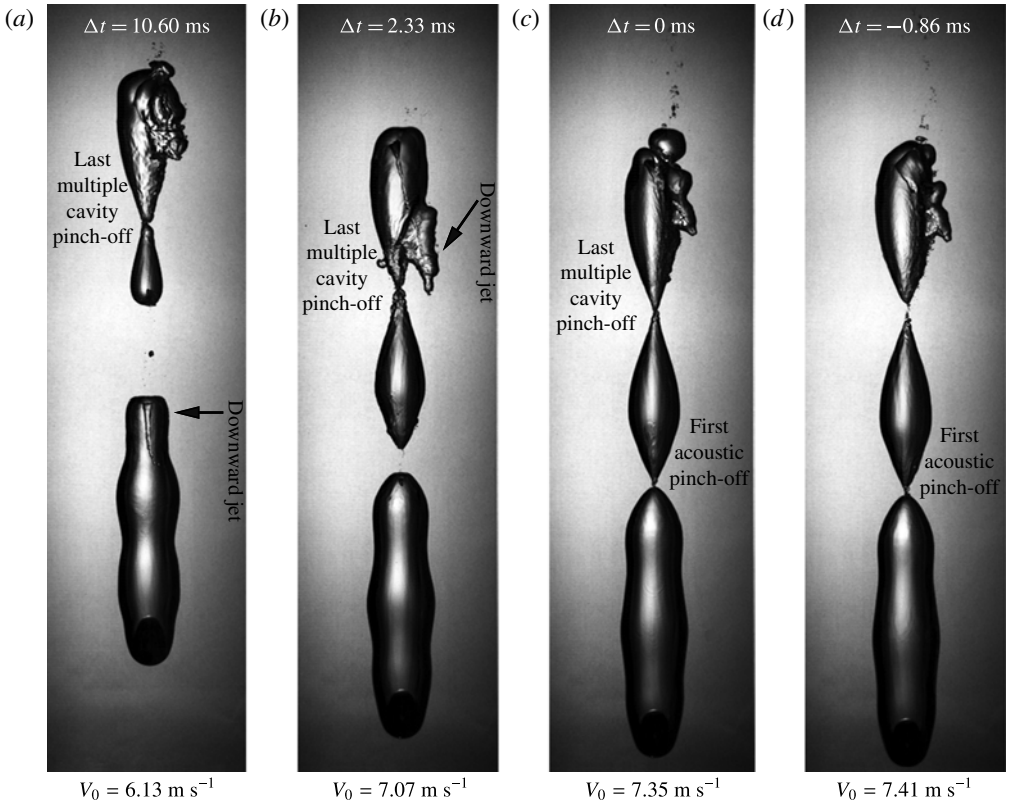


FIGURE 14. Sequence of images showing the time interval Δt (ms) between the last multiple pinch-off and the first acoustic pinch-off produced by guarded surface seal impact of a $D_0 = 25$ mm radius sphere with increasing impact speeds (see the legend) in $D_{tank} = 20$ cm.

ripples, whereas in figure 13(*b*) there are four pinch-offs prior to the image at 129 ms, where only four ripples are observed.

The first acoustic pinch-off depth, which always occurs at the crest of the first acoustic ripple originating from the sphere at position (H) due to the pressure perturbation of the first cavity pinch-off, marks the end of the larger wavelength ripples where $\lambda = O(\text{cm})$. This event abruptly halts the sequential cavity pinch-offs and initiates the cavity shedding regime. Investigating this phenomenon in further detail we present in figure 14, images of the last multiple cavity pinch-off and the first acoustic pinch-off produced by impact of a $D_0 = 25$ mm sphere with increasing impact speeds (see the caption) in a $D_{tank} = 20$ cm tank. Note the near-symmetry of the last multiple pinch-off in figure 14 for $V_0 = 7.35$ m s^{-1} compared with the asymmetric appearance of the acoustic pinch-off. Note also the slanted motion of downward-facing jets which can be reasoned to the occurrence of asymmetrical cavity dynamics as the trajectory of the sphere during its descent begins to deviate slightly from the centre of the narrow container.

In figure 15 we present results for multiple pinch-off depths as (*a*) H_p versus V_0, (*b*) H_p/H versus Fr and times as (*c*) τ(ms) versus Fr for guarded surface seal cavities produced by the impact at various values of ϵ (see the legend). Here (H) is the depth

https://doi.org/10.1017/jfm.2014.35 Published online by Cambridge University Press

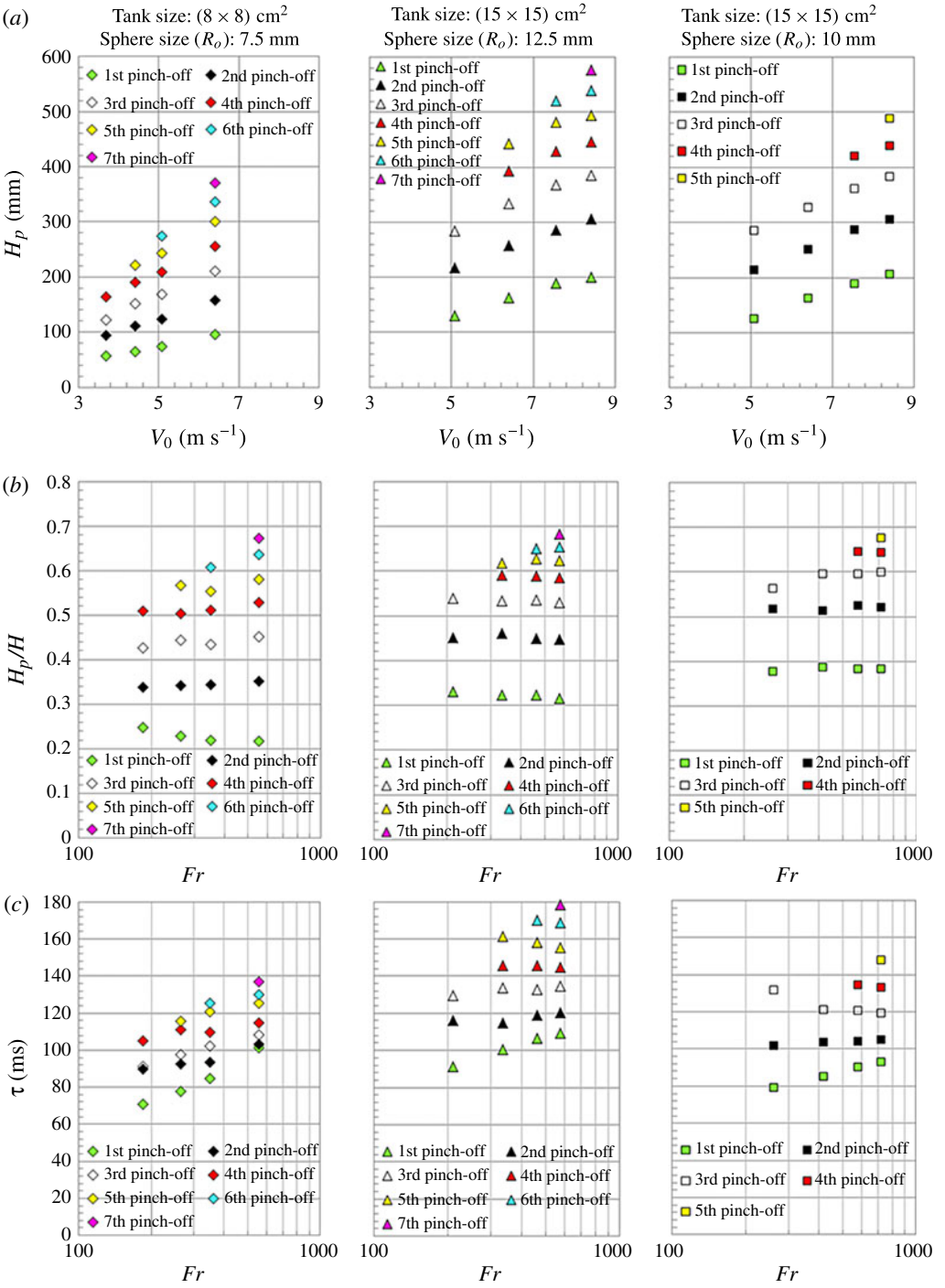


FIGURE 15. (Colour online) Plots of multiple pinch-off depths as (*a*) H_p versus V_0, (*b*) H_p/H versus Fr and times as (*c*) τ (ms) versus Fr for guarded surface seal cavities produced by impact of various sphere radii in the 15×15 cm^2 and 8×8 cm^2 cross-sectional area tanks (see the legend on top), with $\epsilon = 0.19$, 0.166 and 0.133 for columns 1, 2 and 3, respectively.

https://doi.org/10.1017/jfm.2014.35 Published online by Cambridge University Press

of the sphere at the time when the corresponding pinch-off occurs and data points for the first pinch-off have also been included for reference.

From figure 15(*a*) we find H_p values to increase linearly with impact speed for each respective pinch-off, which then leads to scaled depths H_p/H which are independent of the Froude number, as shown in figure 15(*b*). We also observe that the absolute value of H_p/H decreases with increasing wall effects (i.e. increasing ϵ). The pinch-off times plotted in figure 15(*c*) appear independent of impact Froude number for $\epsilon \geqslant 0.133$, but then exhibit a linear dependence on Fr for $\epsilon = 0.19$. Moreover, the time interval between successive pinch-offs gradually diminishes as wall effects increase.

Finally, in figure 16(*a–c*), we present the corresponding data for the acoustic pinch-off as H_a versus V_0, H_a/H versus Fr and τ_a versus Fr, respectively. The scaled values H_a/H are found to be independent of the Froude number for $\epsilon = 0.03$–0.0625 with a constant (mean) value of 0.72 (see the final column in figure 16*b*). However, H_a/H becomes increasingly dependent on the Froude number as the severity of wall effects increases. Similarly, The acoustic pinch-off times plotted in figure 16(*c*) are found to become increasingly dependent on Fr as ϵ increases. Reasonable empirical correlations across the range of ϵ and Fr have been found, which generally involve modifications of the fits to $H_a/H \sim Fr^{1/4}$ and $\tau_a \sim \sqrt{R_0/g}$ with additional prefactors α, β and k (see the caption of figure 16).

4.5. *Cavity shedding*

To highlight the cavity shedding regime described earlier, we present images in figure 17 showing this phenomenon following the acoustic pinch-off. From the images we note the cavity to break systematically similar to observations by Grumstrup *et al.* (2007) but not at every acoustic ripple crest on the cavity surface. This is possibly due to the elongated nature of the cavity caused by strong wall effects and a higher sphere impact speed. We summarize our results for the occurrence of shedding in terms of depths and times versus increasing sphere impact speeds in figure 18(*a*,*b*), respectively. Results for the first acoustic pinch-offs have also been added for comparison. The plots reveal that both depths H_a and times τ_a follow trends similar to that of the first acoustic pinch-off and increase linearly with increase in sphere impact speed.

5. Irregular jet formations

In this section we present some interesting observations for pinch-off and jet formations for impacts with and without wall effects in the absence of surface seal. These include ‘ kinked’ pinch-offs, suppression of the downward facing jets and asymmetric upward facing jets.

Investigating cavity formation and collapse produced by thin circular discs impacts at low speeds of 1 m s^{-1}, Gekle *et al.* (2010) have shown that the air flow through the cavity neck (≈ 0.5 mm in radius) near the pinch-off point, can theoretically reach supersonic speeds. Such high air flow speeds create a Bernoulli suction effect which reduces the pressure at the neck to a minimum of $0.6\,P_a$ when the air reaches a speed of Mach 1. This reduced pressure at the pinch-off point is reported to be strong enough to deform the cavity shape and produce a visible ‘kink’ at the neck (figure 19*a*). In contrast to the air flowing upward through the shrinking neck region, the air at the cavity bottom pulls downwards with the moving disc. This competition for air causes the formation of a stagnation point approximately 5 mm below the pinch-off point. Since the pressure throughout the cavity is roughly equal to P_a and the pinch-off point above has a pressure equal to 0.6 P_a, a high-pressure gradient

https://doi.org/10.1017/jfm.2014.35 Published online by Cambridge University Press

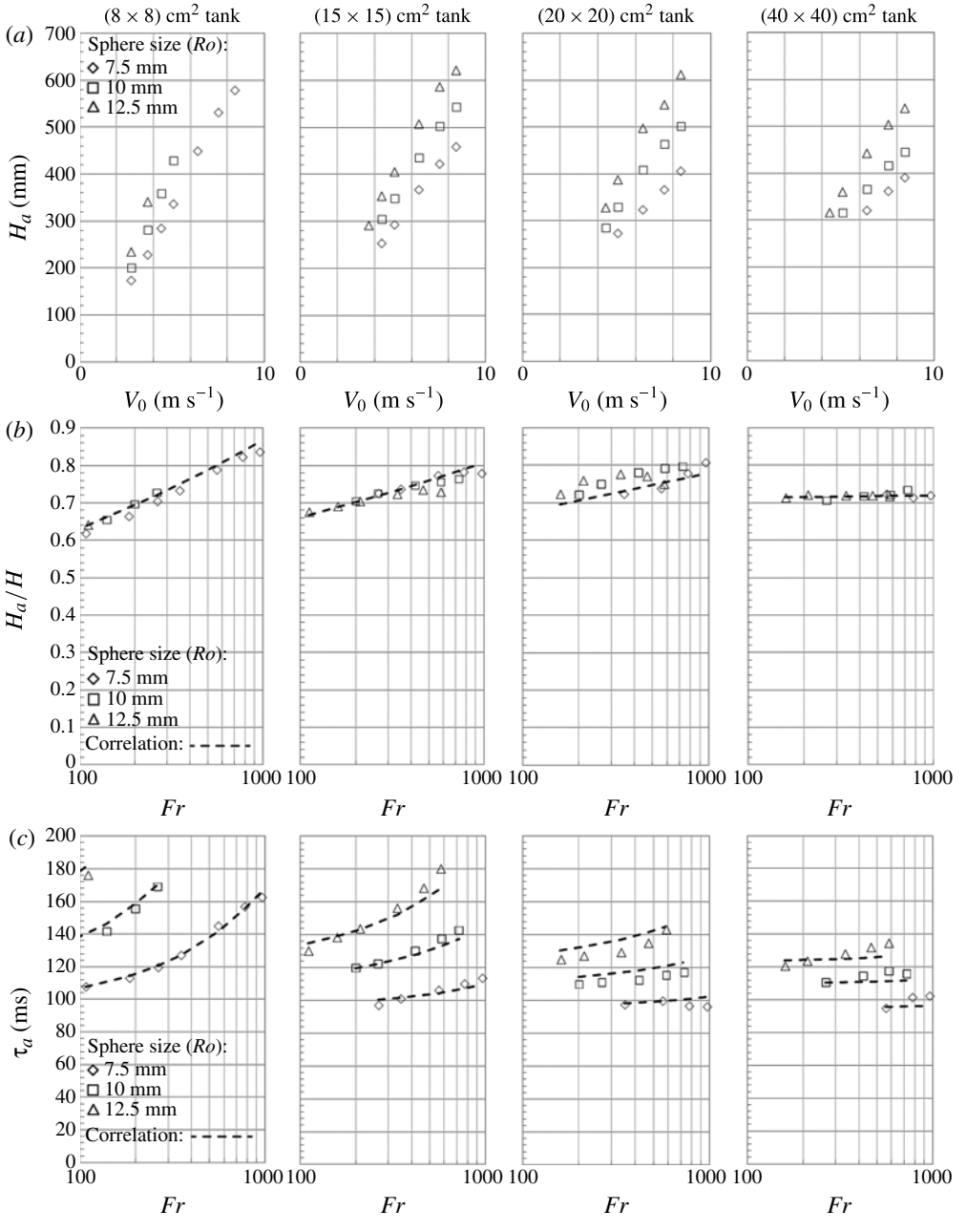


FIGURE 16. Plots of acoustic pinch-off depths and times as (*a*) H_a versus V_0, (*b*) H_a/H versus Fr and (*c*) τ_a versus Fr for guarded impact cavities produced by impact of various sphere radii in four different cross-sectional area tanks (see the legend on top). Fits in (*b*) are averaged for all three sphere sizes and plotted for $H_a/H = \alpha Fr^{(\beta/4)}$, where $\alpha = 0.33$, 0.50, 0.56, 0.72 and corresponding $\beta = 0.56$, 0.26, 0.2, 0 (from left to right). Fits to the curves in (*c*) plot $\tau_a = k\sqrt{R_0/g}$, where the proportionality constant $k = 3.4 + 3/4\epsilon^{2.5}Fr^{0.8}$, $\epsilon = D_0/D_{tank} = 0.0375$–$0.31$ and $Fr = 100$–960.

https://doi.org/10.1017/jfm.2014.35 Published online by Cambridge University Press

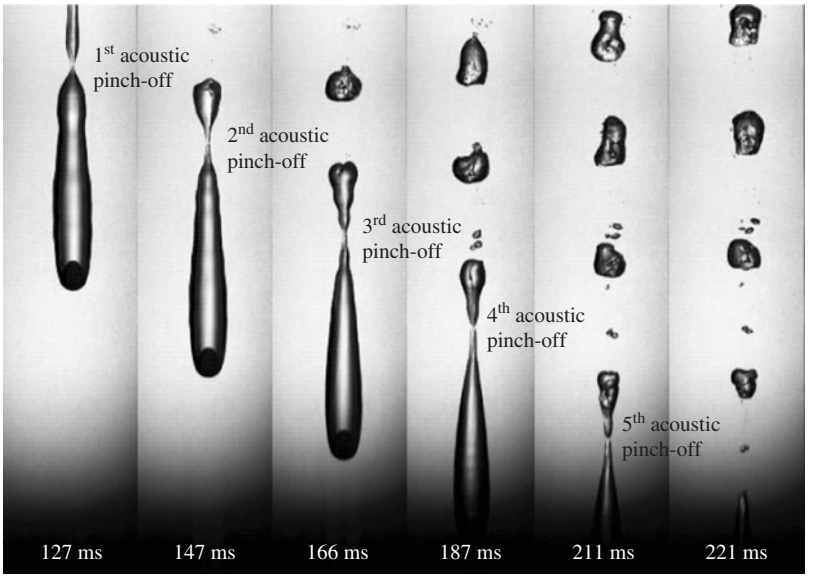


FIGURE 17. Sequence of images showing cavity shedding produced by guarded surface seal impact of a 7.5 mm radius sphere at $V_0 = 6.4$ m s^{-1} in a 8×8 cm^2 cross-sectional area tank. The time from impact has been marked under each image.

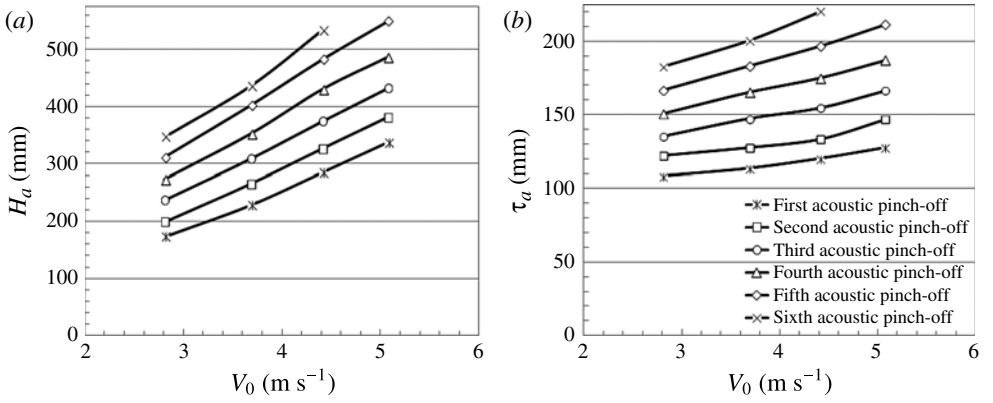


FIGURE 18. Cavity shedding pinch-off depths (*a*) H_a (mm) and times (*b*) τ_a (ms) plotted versus impact speeds V_0 of a 7.5 mm radius sphere colliding with the free surface in a 8×8 cm^2 cross-sectional area tank with guarded surface seals.

is created. This results in a very strong air flow capable of drawing liquid with it which pulls the neck upwards (≈ 0.5 mm) in the final moments of collapse. We also note that since the cavity interfaces can never be perfectly smooth, due to inevitable contact line pinning around the sphere, there are azimuthal disturbances which become amplified as the neck radius diminishes (see supplementary movie 3).

In the experiments with wall effects and guarded surface seals carried out in our study, the effects reported by Gekle *et al.* (2010) are enhanced as observed in figure 19(*b,c*). Here we present full-view images (*b*) and corresponding close-ups (*c*) of the first cavity pinch-off produced by a guarded impact (see the caption for details).

https://doi.org/10.1017/jfm.2014.35 Published online by Cambridge University Press

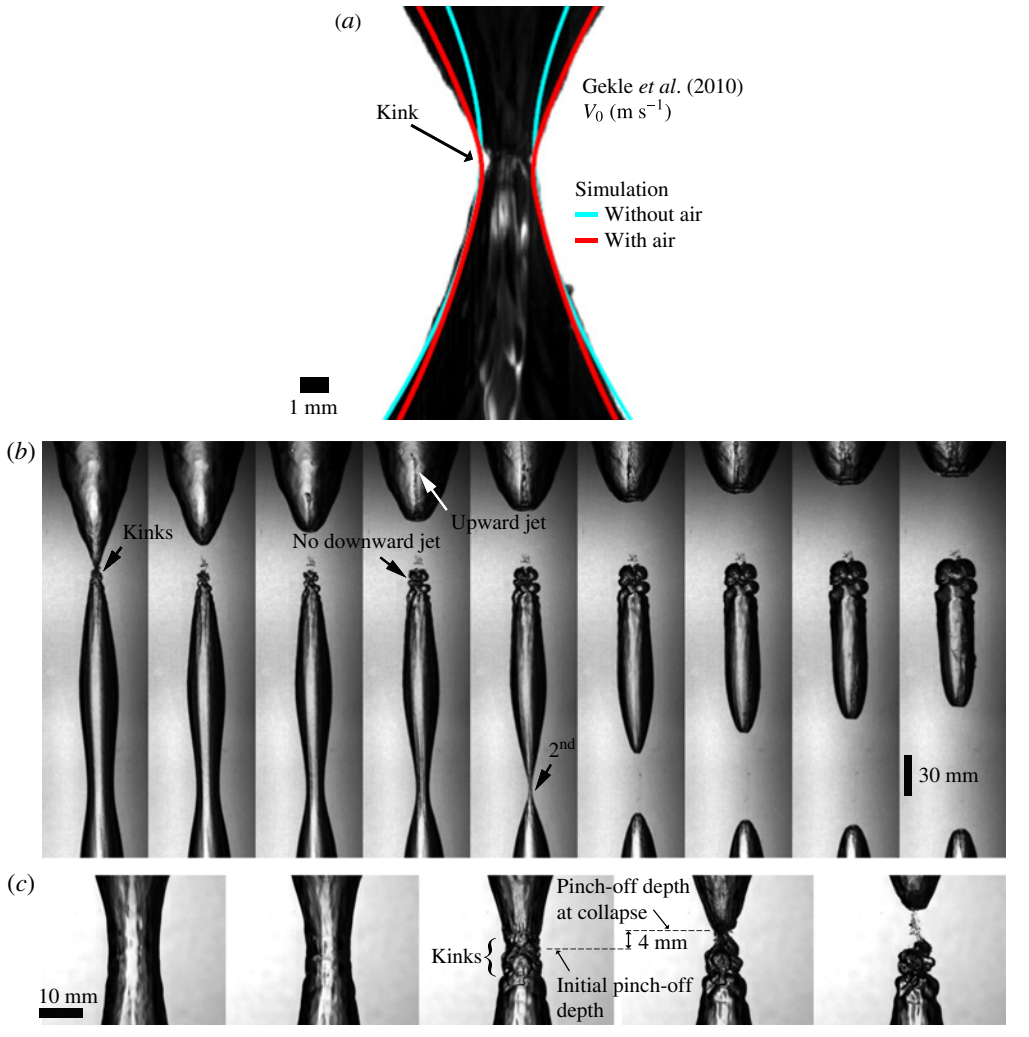


FIGURE 19. (Colour online) (*a*) Image from Gekle *et al.* (2010) showing a kink at the cavity pinch-off point created by a 2 cm radius disc for $V_0 = 1$ m s^{-1}. (*b*) Full-view ($\Delta t = 2.66$ ms) and (*c*) close-up images ($\Delta t = 1$ ms) of the first cavity pinch-off point produced by the guarded impact of a $D_0 = 20$ mm sphere at $V_0 = 8.4$ m s^{-1} in $D_{tank} = 20$ cm. The first images in (*b*) and (*c*) are taken at 64 ms and 75 ms after impact, respectively.

Images in (*c*) not only show larger 'kinks' at the necking region compared with that by Gekle *et al.* (2010) but also a noticeably larger upward movement of the neck (≈ 4 mm) prior to collapse. We postulate that the air flow mechanism proposed by Gekle *et al.* (2008) is enhanced for our case since we have an elongated cavity and multiple, simultaneously necking regions, each of which may act to strengthen the air flow through the first wave crest, thus leading to the kink observed in figure 19(*c*). This process also acts to suppress the downward-facing jet (see figure 19*b*) and is repeated at subsequent pinch-offs.

In figure 20 we present snapshots of upward facing jet structures obtained by guarded impacts of a $D_0 = 20$ mm radius sphere at various speeds (see the legend)

https://doi.org/10.1017/jfm.2014.35 Published online by Cambridge University Press

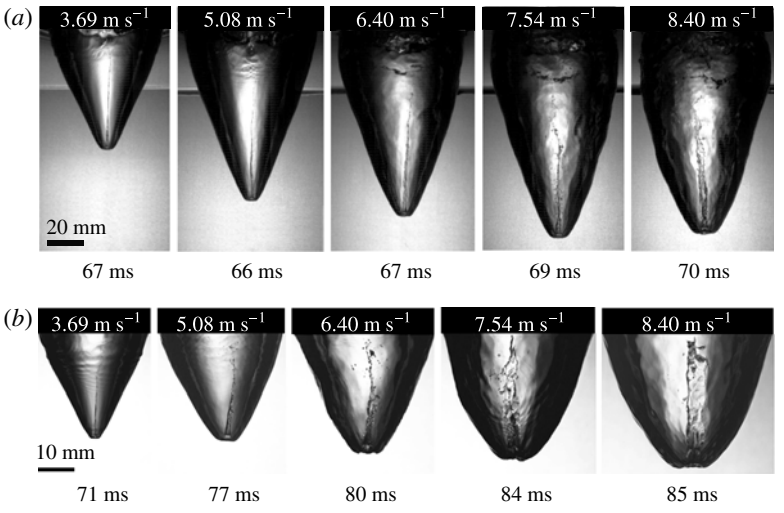


FIGURE 20. Snapshots of upward traveling jet structures following the first pinch-off of the cavity produced by guarded surface seal impacts of a 10 mm radius sphere at $V_0 = 3.69, 5.08, 6.40, 7.54$ and 8.4 m s^{-1} (starting from the left). In (*a*) wall effects are insignificant (50×50 cm^2 tank) and in (*b*) wall effects are significant (20×20 cm^2 tank). The time from impact has been marked under each respective image.

in (*a*) $D_{tank} = 50$ cm and (*b*) $D_{tank} = 20$ cm. A close examination reveals the jet structures to transition from an axisymmetric streamlined configuration to an irregular, asymmetric structure with increase in V_0. This transition is noted to occur starting at earlier impact velocities as wall effects become important. Interestingly, at the highest impact velocity of $V_0 = 8.40$ m s^{-1} in (*a*) and (*b*), the jet evolves into a 'flat' structure. We illustrate this structure in further detail in figure 21, showing a sequence of images from the same realization as the final image in figure 20(*b*). From these images we clearly see the formation of the flat jet, which maintains this structure as it travels upwards through the open cavity. The proximity of the cavity to the square sided tank walls is likely to cause the asymmetry in cavity dynamics resulting in the irregular and flat jet structures observed in figure 20(*b*). In addition, since the sphere trajectory during the fall tends to deviate more and at earlier impact speeds from the centre of smaller cross-sectional area tanks, the induced asymmetry is larger resulting in earlier and more obvious irregularities. While both of these phenomenon can significantly affect the symmetry of cavity dynamics in the presence of prominent wall effects, only the latter is expected to hold true in the absence of wall effects (figure 20*a*).

6. Conclusions

We have presented an experimental study of cavity formation produced by hydrophobic sphere impacts onto water for an extended regime of Froude numbers ($18 < Fr < 960$) compared with that by Duclaux *et al.* (2007) for ($10 < Fr < 330$). We used conical-shaped splash-guards to prevent the surface splash from converging above the centre and producing droplets that collide with the cavity interface formed beneath, which typically leads to distortion of the cavity walls at Froude numbers $Fr > O(100)$. Thus, we were able to prohibit the surface seal phenomenon and study

https://doi.org/10.1017/jfm.2014.35 Published online by Cambridge University Press

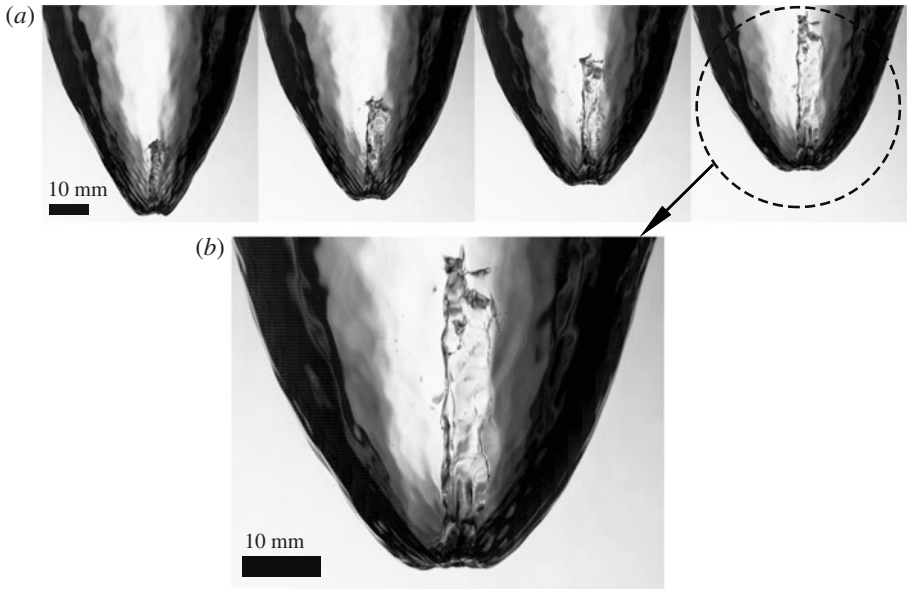


FIGURE 21. (*a*) Images at 1 ms interval showing the evolution of a flat jet produced by guarded surface seal impact of a 10 mm radius sphere at $V_0 = 8.4$ m s^{-1} in a 20×20 cm^2 cross-sectional tank. The first image is taken at 81.6 ms after impact. (*b*) Close-up views of the final image in (*a*), taken at 84.6 ms from impact. See also supplementary movie 3.

the ensuing undisturbed cavity dynamics. Guarded impact cavities without surface seal were also studied in the presence of wall effects by systematically varying the tank size and sphere diameter.

The scaled depth and time of primary cavity pinch-off for negligible wall effects, even in the extended regime of Froude numbers, were found to be in reasonable agreement with the theoretical prediction of $H_p/H = 1/2$ and the scaling $\tau = 2.06\sqrt{R_0/g}$ provided by Duclaux *et al.* (2007). The values were found to decrease significantly if the surface seals were not prevented.

Guarded surface seal impacts in the presence of wall effects, created using constrained geometries resulted in the formation of surface undulations along the cavity interface with typical wavelengths, $\lambda = O(\text{cm})$. The wavelength was observed to increase with increasing impact speed and decreased with increasing depth and severity of wall effects. The crests of these undulations acted as favourable points for cavity closure and lead to the formation of multiple cavity pinch-offs. The significance of surface tension in this phenomenon was examined by performing experiments with perfluorohexane, leading to much smaller wavelengths than in water, despite only a slight change in sphere velocity due to the increased liquid density. Furthermore, PIV experiments showed these undulations to have a stationary nature with respect to the lab frame.

By systematically varying the sphere-to-tank diameter ratio, ϵ, we observed that both the pinch-off depth and time become strong functions of sphere size and impact speed. However, for the largest tanks with $D_{tank} = 40$ and 50 cm, we noted negligible wall effects and thus concluded that geometrical constraints became important for $\epsilon = D_0/D_{tank} > 0.075$. For the smallest tanks, where surface undulations were present above

https://doi.org/10.1017/jfm.2014.35 Published online by Cambridge University Press

the first cavity pinch-offs, we found distinct regimes separated by pronounced jumps whereby the scaled pinch-off depths initially decrease, then sharply increase as the impact speed increases.

Similar to observations by Grumstrup *et al.* (2007), pressure perturbations caused by the occurrence of multiple pinch-offs were found to simultaneously generate distinct waves at the sphere surface. These acoustic waves had wavelengths $\lambda_a = O(D_{sphere})$ and are thus distinct from the larger undulations observed before the primary pinch-off.

Acoustic wave crests were also found to act as favourable points for cavity closure and hence formed multiple pinch-off points, which was termed the 'cavity shedding regime'. The first acoustic pinch-off was always found to occur at depth H below the free surface, where H is the sphere depth when primary pinch-off occurs. The first acoustic pinch-off depths scaled as H_a/H and times τ_a were found to gradually become an increasing function of the Froude number with increase in wall effects.

The 'kinks' observed by Gekle *et al.* (2010) were found to be significantly enhanced in the presence of wall effects, producing distinct 'kinks' especially at first cavity pinch-off points which were also shown to move a comparatively large upward distance of up to ≈ 4 mm prior to collapse. We speculated that this was due to the presence of multiple undulation crest necking regions due to wall effects which then aid the upward air flow through the first pinch-off region and thus cause a larger local pressure gradient. The air flow direction at the primary pinch-off and subsequent multiple pinch-offs then completely suppresses the downward facing jet, whilst the upward facing jets were found to undergo a transition from symmetrical to irregular, asymmetric jets.

Extensions of the analytical model presented by Duclaux *et al.* (2007), in order to correct for wall effects and account for multiple pinch-off points is the subject of ongoing work. In addition, the use of circular containers to impose wall effects without influencing the axisymmetry of guarded surface seal impact cavities can be a potential research topic for future studies.

Acknowledgement

We thank Erqiang Li for assistance during the experimental work.

Supplementary movies

Supplementary movies are available at http://dx.doi.org/10.1017/jfm.2014.035.

REFERENCES

ARISTOFF, J. M. & BUSH, J. W. M. 2009 Water entry of small hydrophobic spheres. *J. Fluid Mech.* **619**, 45–78.

ARISTOFF, J. M., TRUSCOTT, T., TECHET, A. H. & BUSH, J. W. M. 2010 The water entry of decelerating spheres. *Phys. Fluids.* **22**, 032102.

BELL, G. E. 1924 On the impact of a solid sphere with a fluid surface. *Phil. Mag. J. Sci.* **48**, 753–765.

BERGMANN, R., VAN DER MEER, D., VAN DER BOS, A. & LOHSE, D. 2009 Controlled impact of a disk on a water surface: cavity dynamics. *J. Fluid Mech.* **633**, 381–409.

BIRKHOFF, G. & ISAACS, R. 1951 Transient cavities in air water entry, *Tech. Rep.* 1490 Navord Rep.

BURLEY, R. 1992 Air entrainment and the limits of coatability. *JOCCA* **75** (5), 192–202.

https://doi.org/10.1017/jfm.2014.35 Published online by Cambridge University Press

DUCLAUX, V., CAILLE, F., DUEZ, C., YBERT, C., BOCQUET, L. & CLANET, C. 2007 Dynamics of transient cavities. *J. Fluid Mech.* **591**, 1–19.

DUEZ, C., YBERT, C., CLANET, C. & BOCQUET, L. 2007 Making a splash with water repellency. *Nat. Phys.* **3**, 180–183.

DI FELICE, R. 1996 A relationship for the wall effect on the settling velocity of a sphere at any flow regime. *Int. J. Multiphase Flow* **22**, 527–533.

GEKLE, S., GORDILLO, J. M., VAN DER MEER, D. & LOHSE, D. 2009 High-speed jet formation after solid object impact. *Phys. Rev. Lett.* **102**, 034502.

GEKLE, S., PETERS, I. R., GORDILLO, J. M., VAN DER MEER, D. & LOHSE, D. 2010 Supersonic air flow due to solid–liquid impact. *Phys. Rev. Lett.* **104**, 024501.

GEKLE, S., VAN DER BOS, A., BERGMANN, R., VAN DER MEER, D. & LOHSE, D. 2008 Noncontinuous Froude number scaling for the closure depth of a cylindrical cavity. *Phys. Rev. Lett.* **100**, 084502.

GILBARG, D. & ANDERSON, R. 1948 Influence of atmospheric pressure on the phenomena accompanying the entry of spheres into water. *J. Appl. Phys.* **19**, 127–139.

GLASHEEN, J. W. & MCMAHON, T. A. 1996 A hydrodynamical model of locomotion in the basilisk lizard. *Nature* **380**, 340–342.

GRUMSTRUP, T., KELLER, J. B. & BELMONTE, A. 2007 Cavity ripples observed during the impact of solid objects into liquids. *Phys. Rev. Lett.* **99**, 114502.

LEE, M., LONGORIA, R. G. & WILSON, D. E. 1997 Cavity dynamics in high-speed water entry. *Phys. Fluids.* **9** (3), 540–550.

MALLOCK, A. 1918 Sounds produced by drops falling on water. *Proc. R. Soc. Lond.* A **95**, 138–143.

MARSTON, J. O., VAKARELSKI, I. U. & THORODDSEN, S. T. 2011 Bubble entrapment during sphere impact onto quiescent liquid surfaces. *J. Fluid Mech.* A **680**, 660–670.

MARSTON, J. O., VAKARELSKI, I. U. & THORODDSEN, S. T. 2012*a* Cavity formation by the impact of Leidenfrost spheres. *J. Fluid Mech.* **699**, 465–488.

MARSTON, J. O., ZHU, Y., VAKARELSKI, I. U. & THORODDSEN, S. T. 2012*b* Deformed liquid marbles: freezing drop oscillations with powders. *Powder Tech.* **228**, 424–428.

MAY, A. 1951 Effect of surface condition of a sphere on its water-entry cavity. *J. Appl. Phys.* **22**, 1219–1222.

MAY, A. 1952 Vertical entry of missiles into water. *J. Appl. Phys.* **22**, 1362–1372.

MAY, A. & HOOVER, W. R. 1963 A study of the water-entry cavity. Unclassified NOLTR 63-264. United States Naval Ordinance Laboratory, White Oak, MD.

MAY, A. & WOODHULL, J. C. 1948 Drag coefficients of steel spheres entering water vertically. *J. Appl. Phys.* **19**, 1109–1121.

MAY, A. & WOODHULL, J. C. 1950 The virtual mass of a sphere entering water vertically. *J. Appl. Phys.* **21**, 1285–1289.

METZGER, M. A. 1981 A computer program for modeling water entry cavity performance and comparison of predicted with observed cavities. Naval Surface Weapons Center, Silver Springs, MD, Report No. NSWC/TR-81-59.

RAMSAUER, C. & DOBKE, G. 1927 Die Bewegungserscheinungen des Wassers beim Durchgang schnell bewegter Kugeln. *Ann. Phys. Lpz.* **389**, 697–720.

RICHARDSON, E. G. 1948 The impact of a solid on a liquid surface. *Proc. Phys. Soc.* **61**, 352–367.

ROSELLINI, L., HERSEN, F., CLANET, C. & BOCQUET, L. 2005 Skipping stones. *J. Fluid Mech.* **543**, 137–146.

ROYER, J. R., CORWIN, E. I., CONYERS, B., FLIOR, A., RIVERS, M. L., ENG, P. J. & JAEGER, H. M. 2008 Birth and growth of a granular jet. *Phys. Rev.* E **78**, 011305.

SHI, H. H., ITOH, M. & TAKAMI, T. 2000 Optical observation of the supercavitation induced by high-speed water entry. *Trans. ASME* **122**, 806–810.

THORODDSEN, S. T., ETOH, T. G., TAKEHARA, K. & TAKANO, Y. 2004 Impact jetting by a solid sphere. *J. Fluid Mech.* **499**, 139–148.

THORODDSEN, S. T., ETOH, T. G. & TAKEHARA, K. 2008 High-speed imaging of drops and bubbles. *Annu. Rev. Fluid Mech* **40**, 257–285.

https://doi.org/10.1017/jfm.2014.35 Published online by Cambridge University Press

TRUSCOTT, T. T. & TECHET, A. H. 2009 Water entry of spinning spheres. *J. Fluid Mech.* **625**, 135–165.

VAKARELSKI, I. U., MARSTON, J. O., CHAN, D. Y. C. & THORODDSEN, S. T. 2011 Drag reduction by Leidenfrost vapor layers. *Phys. Rev. Lett.* **106**, 214501.

VAKARELSKI, I. U., PATANKAR, N. A., MARSTON, J. O., CHAN, D. Y. C. & THORODDSEN, S. T. 2012 Stabilization of Leidenfrost vapour layer by textured superhydrophobic surfaces. *Nature* **489**, 274–277.

VON KANN, S., JOUBAUD, S., CABALLERO-ROBLEDO, G. A., LOHSE, D. & VAN DER MEER, D. 2010 Effect of finite container size on granular jet formation. *Phys. Rev.* E **81**, 041306.

WORTHINGTON, A. M. 1908 *A study of splashes*. Longmans Green.

WORTHINGTON, A. M. & COLE, R. S. 1897 Impact with a liquid surface, studied by the aid of instantaneous photography. *Phil. Trans. R. Soc. Lond.* A **189**, 137–148.

WORTHINGTON, A. M. & COLE, R. S. 1900 Impact with a liquid surface, studied by the aid of instantaneous photography: paper 2. *Phil. Trans. R. Soc. Lond.* A **194**, 175–1499.

https://doi.org/10.1017/jfm.2014.35 Published online by Cambridge University Press